ELECTROLYTE-GATED FIELD-EFFECT TRANSISTORS FOR SENSING AN ALZHEIMER'S DISEASE HALLMARK

S. Ruiz-Molina, S. Ricci, S. Casalini and M. Mas-Torrent

Institut de Ciència de Materials de Barcelona (ICMAB-CSIC), Campus UAB, 08193 Bellaterra, Spain

INTRODUCTION

Electrolyte-Gated Organic Field Effect Transistors (EGOFETs) have been investigated recently as a useful means for biological sensing. Their working principle is based on converting a chemical event into a readable electrical signal. These devices can be prepared at low cost and on flexible substrates and are ultrasensitive due to the amplification ability of transistors.

In this study we report the use of EGOFETs in order to develop a device that can respond to a biomarker related to Alzheimer's disease: $A\beta_{1-40}$ peptide, whose aggregation in oligomers is believed as major toxic effect in this pathology.

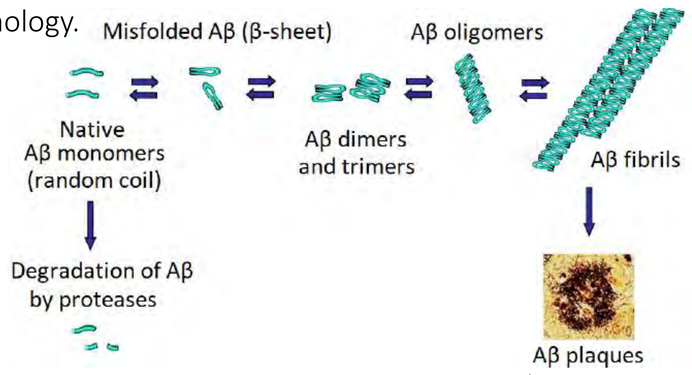

-Aβ peptide aggregation process from monomers to fibrils/ diffuse plaques-

OBJECTIVES

The main objective of this work is the development of a label-free immunosensor based on EGOFETs for study the $A\beta_{1-40}$ aggregation.

To achieve this goal, an optimization of the biofunctionalization protocol of the gate electrode and a study of the kinetics of $A\beta_{1-40}$ aggregation employing both electrochemistry and EGOFET measurements were performed.

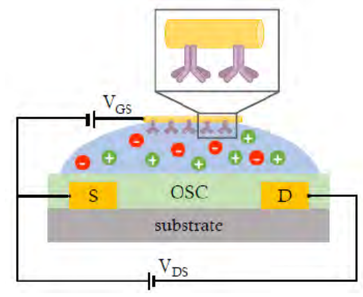

-EGOFET used as a biosensor with a functionalised gate electrode with antibodies-

EGOFET FABRICATION AND CHARACTERIZATION

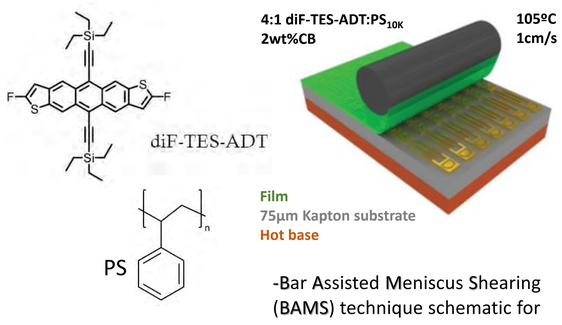

-Bar Assisted Meniscus Shearing (BAMS) technique schematic for organic semiconductor deposition-

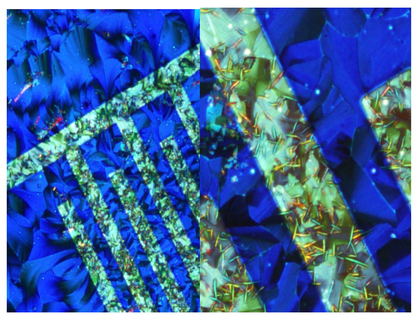

-Optical polarized microscopy images of diF-TES-ADT:PS thin films-

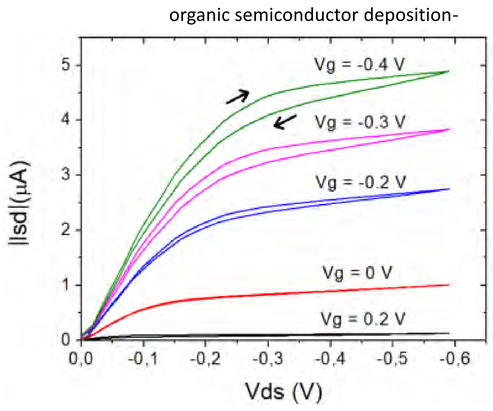

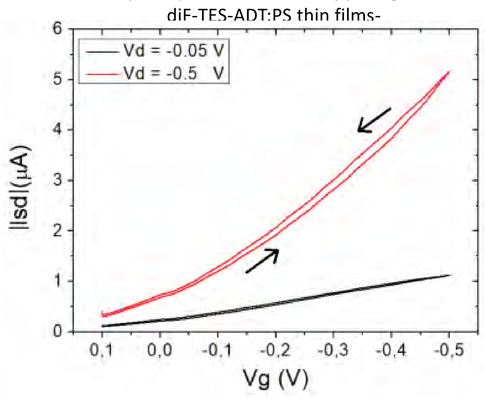

a) Output characteristics and b) transfer characteristics of the EGOFETs based on diF-TES-ADT:PS (10 mm·s^{-1}) using PBS 1X (pH=7.4) as electrolyte.

EGOFET based in diF-TES-ADT:PS_{10K} (4:1) blend deposited by BAMS technique were successfully fabricated. Good crystallinity, environmental stability and correct device operation using PBS 1X as electrolyte were obtained.

GATE ELECTRODE FUNCTIONALIZATION

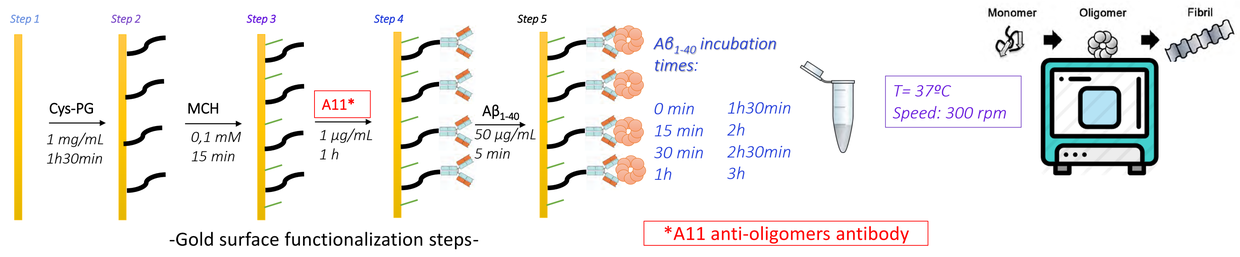

-Gold surface functionalization steps-

*A11 anti-oligomers antibody

ELECTROCHEMICAL CHARACTERIZATION

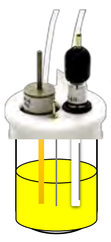

-Three- electrode configuration cell-
WE: Au wire
RE: Ag/AgCl
CE: Pt wire
Redox marker: $[Fe(CN)_6]^{-3/-4}$

Redox marker solution:
$5\ mM\ [Fe(CN)_6]^{-3/-4}$
100 mM KCl
50 mM phosphate salt
pH=7

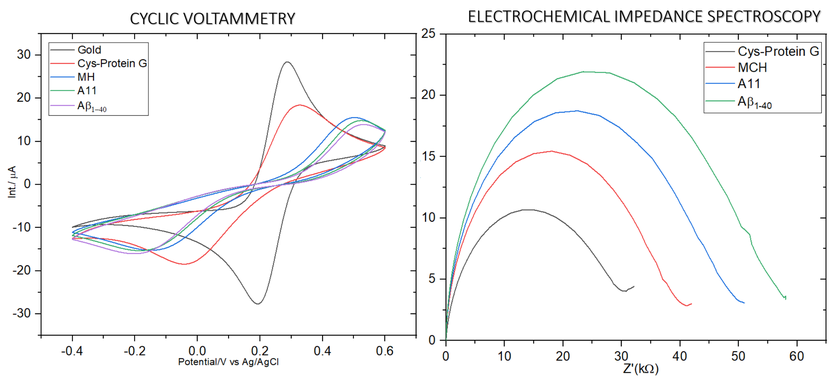

-CV measurements (left) and EIS measurements (right) over each functionalisation step using $[Fe(CN)_6]^{3-/4-}$ as a redox mediator-

The increase in Rct in each functionalization step shows that a successful gate functionalization process was achieved to adhere A11 antibodies, which are specific to $A\beta_{1-40}$ oligomers.

SENSING RESPONSE — ELECTROCHEMICAL CHARACTERIZATION

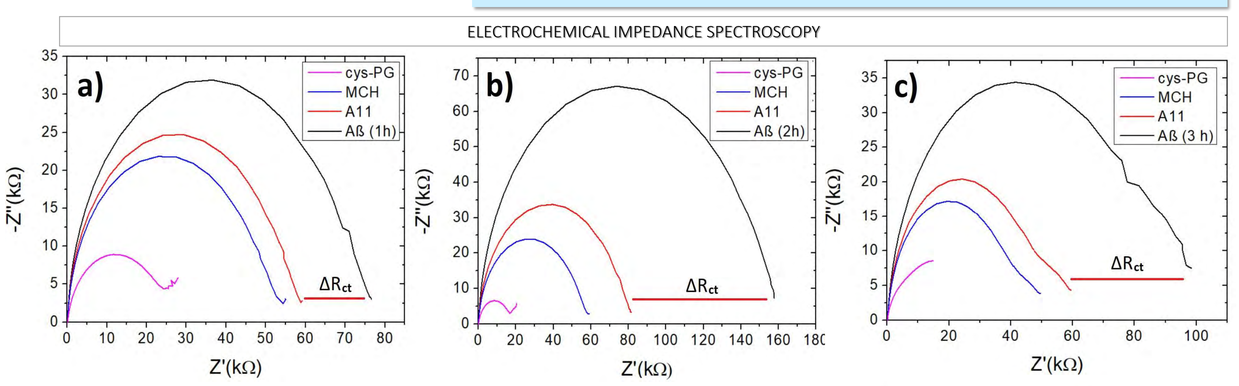

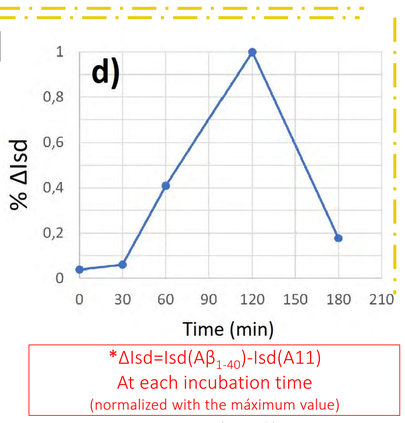

*ΔIsd=Isd($A\beta_{1-40}$)-Isd(A11)
At each incubation time
(normalized with the máximum value)

-EIS measurements for **a)** 1 hour, **b)** 2 hours and **c)** 3 hours $A\beta_{1-40}$ incubation times. Figure **d)** shows the comparison between the ΔRct* between different incubation times-

*ΔRct=Rct($A\beta_{1-40}$)-Rct(A11)
At each incubation time

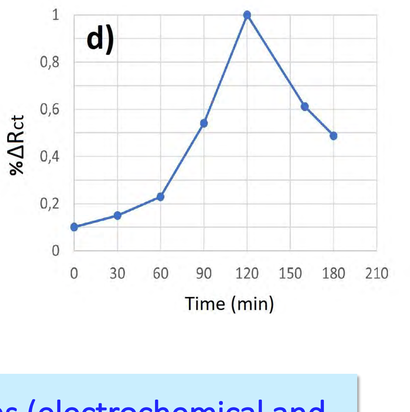

SENSING RESPONSE — EGOFET CHARACTERIZATION

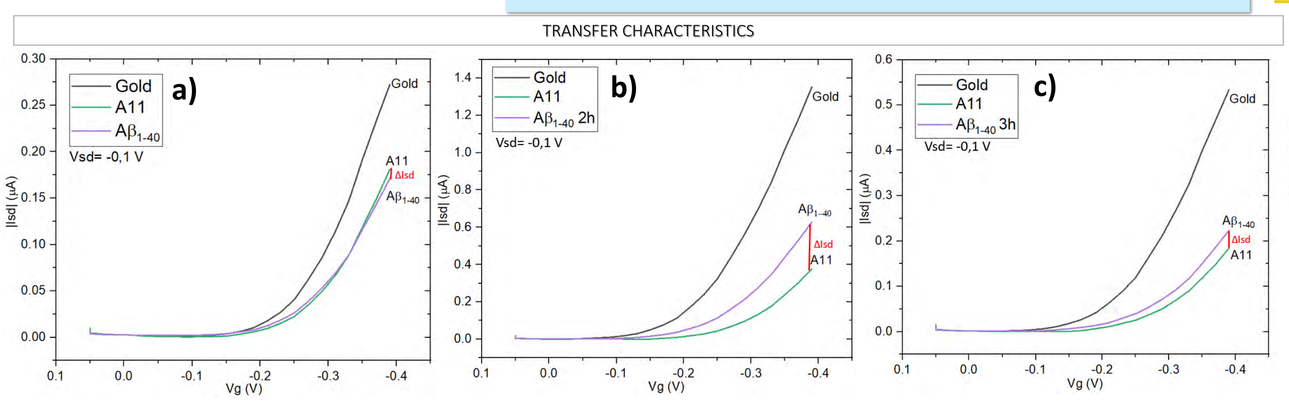

-Transfer measurements for **a)** 1 hour, **b)** 2 hours and **c)** 3 hours, Aβ1-40 incubation times. Figure **d)** shows the comparison between the change in the maximum current (ΔIsd*) between different incubation times-

In both characterizations (electrochemical and EGOFET), the maximum concentration of oligomers is observed at an incubation time of 2 hours.

Conclusions

In this work, an EGOFET immunosensor has been successfully fabricated and used to study the kinetics of $A\beta_{1-40}$ aggregation.
Some conclusions can be drawn:

- The functionalization protocol of the Au electrode has been successfully applied to adhere antibodies to its surface.
- $A\beta_{1-40}$ maximum oligomer species is found at 2 hours incubation time in both electrochemical and EGOFET characterization.

As future work, more experiments regarding the reproducibility of the EGOFET characterization will be performed.

As a general conclusion, EGOFETs based biosensors have demonstrated to be a strong contender on the field by offering an ultrasensitive, highly selective, label-free transduction mechanism for biorecognition events. This new technology could elevate the field of point-of-care diagnostics, allowing for an early diagnostic and treatments.

References:
[1] M. Berto, E. Vecchi, L. Baiamonte, C. Condò, M. Sensi, M. Di Lauro, M. Sola, A. De Stradis, F. Biscarini, A. Minastra, C. A. Bartolotti, *Sensors & Actuators: B. Chemical,* 281 (2019) 150.
[2] S. Ricci, S. Casalini, V.Parkula, P Greco, F. Biscarini, M. Mas-Torrent, *Biosensors and Bioelectronics*, 167 (2020) 112433.
[3] A. J. Veloso, A. M. Chow, H. V. S. Ganesh, N. Li, D. Dhar, D. C. H. Wu, S. Mikhaylichenko, I. R. Brown, K. Kerman, *Anal. Chem.,* 86 (2014) 4901.
[4] I. Temiño, F. G. Del Pozo, M.R. Ajayakumar, S. Galindo, J. Puigdollers, M. Mas-Torrent, Adv. Mater. Technol., 1 (2016) 1600090.

Acknowledgements:

This work was funded by the Spanish Ministry with the Project GENESIS PID2019-111682RB-I00 and through the "Severo Ochoa" Programme for Centers of Excellence in R&D (FUNFUTURE CEX2019-000917-S).

Electrothermal modeling of Mo/Au Transition-Edge Sensors

M.Mas[1], C.Pobes[2], A.Camón[2], J.Bolea[3], P.Strichovanec[2], L.Fàbrega[1]

[1]ICMAB-CSIC, Bellaterra (Spain) [2]INMA, CSIC-Universidad de Zaragoza, Zaragoza (Spain) [3] Centro Universitario de la Defensa, Zaragoza (Spain)

SUMMARY

Transition-Edge Sensors (TES) are radiation detectors working at cryogenic temperatures [1,2] (~ 100 mK) having capability for sensing very small amounts of energy coming from X-rays (~ few keV), for example, with superior sensitivity (~ 1 eV). TES can even detect single photons and measure their energy with high accuracy. TES are used in Astrophysics and Cosmology applications, as well as in Nanotechnology and Quantum Technologies. TES have already been implemented on telescopes and in a future (2032) the detector of the high spectral resolution instrument of the next telescope of X-rays from the European Spatial Agency (ESA), Athena, will be constituted by TES [3]. TES are microcalorimeters (electrothermal devices) made of a superconducting (SC) thin film (or bilayer). They take advantage of the steep resistive transition of the SC material between the normal and superconducting states (typically a few mK). This is what makes TES very sensitive to incoming radiation.

TES performances (their spectral energy resolution and response time) depend on TES parameters, which are extracted from fits to the measured complex impedance Z(ω); these fits require an electrothermal model of the TES, that is, knowing the number of relevant thermal blocks and their configuration. Therefore, in order to optimize TES performances and improve them, electrothermal modeling plays a key role. Usually, TES parameters are extracted by using the simplest electrothermal model, that is, considering the TES constituted by a single thermal block (1 TB). This is, though, an approximation even when no absorber is present. In this work we develop fits to Z(ω) of bare TES considering different configurations with 2 thermal blocks (2 TBs) and analyze when the second TB becomes relevant, and what is its impact on basic TES parameters. We report on the results obtained so far, including a critical analysis of fits reliability and the TES size effects on the TES thermal parameters, which in the end should help us to identify the present TBs.

TES PHYSICS and OPERATION

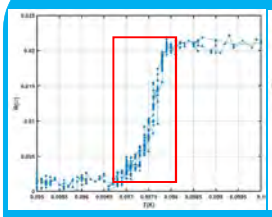

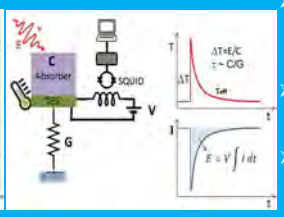

- TESs have an absorber to collect photons and convert the radiation energy into thermal energy (thermalization process) to be sensed by the superconducting part of TES (it heats).
- TES is in thermal contact with a bath, at a cryogenic temperature (T_{bath}) through a thermal link (a membrane for X-rays).
- TES resistance increases when a photon is absorbed, and since voltage is kept constant, that produces an inverse peak of current (this is what we measure).

Operation mode: negative electrothermal feedback [1]. TES is voltage-biased and thus self-heated above T_{bath}. Working at constant bias voltage enables the TES to return to its working point (after an excitation) and makes it stable thanks to the so-called Negative Electrothermal feedback: Joule power is inversely proportional to resistance ($P_J = V^2/R$) so, if T increases, so does R, and P_J is reduced. Thus, the TES cools down and returns to its equilibrium position.

Analyzed devices:

- Membrane (Si_3N_4) 0.5 μm, 250x250μm
- Mo/Au bilayers with Nb/Mo contacts
- R_n (normal resistance) = 24 mΩ;

Bilayer T_c (transition critical temperature): $T_{ci} \approx 92$ mK

5 devices with sizes (w (width) x L (length), μm²):
25x25, 25x50, 25x75, 25x100, 120x120

Dark characterization performed in Kelvinox dilution refrigerator. It included:

- I-V curves and Z(ω) measurements performed under DC bias at T_{bath} = 50 mK.

ELECTROTHERMAL MODELING, TES performances and TES parameters

TES performances: (1) Spectral energy resolution (δE) and (2) Response time (τ_{eff}) are determined by **TES parameters*: (1) α and β**: logarithmic derivatives of TES resistance to temperature and current and **(2) C** and **G** (g's): heat capacity/ies and thermal conductance/s.

$$\delta E_{FWHM} = 2\sqrt{2\ln 2}\sqrt{\frac{4k_B T_0^2 C}{\alpha}}\sqrt{\frac{nF(T_0,T_{bath})\xi(I_0)}{1-(T_{bath}/T_0)^n}}$$

*Obtained by fitting Z(ω): TES complex impedance data + data from I-V curves

$$\tau_{eff} = \frac{C}{G}\frac{1+\beta+R_L/R_0}{1+\beta+R_L/R_0+(1-R_L/R_0)\mathcal{L}_I} \quad \text{where } \mathcal{L}_I \equiv \frac{P_{J_0}\alpha}{GT_0} \quad \text{And } R_L = R_{SH} + R_{PAR}^{**}$$

***Shunt resistance (connected in parallel to TES to bias it at constant voltage) + parasitic resistance of the electrical circuit where TES is, respectively.*

Z(ω)'s fitting formulae and expressions from the electrothermal modeling provided by [4] according to a thermal block(s) model (1 TB, 2 TB). Z(ω) fits performed with MatLab: Least Squares (LS) method.

Thermal block models and configurations

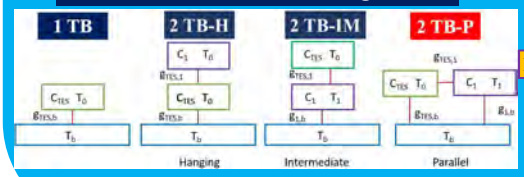

Z(ω) fits → Fitting parameters → TES parameters

5 fitting parameters to give… 6 (4) TES parameters when 2 TB* (1 TB) is used: (α, β, 2 C's, 2 g's)

Block configuration*

Additional hypothesis required*

FITS of Z(ω): 1 TB and 2 TB

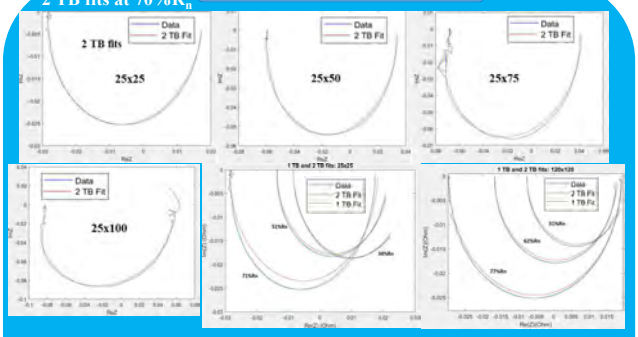

- Even for these bare TES Z(ω) clearly deviates from the expected semicircular shape of 1 TB. 2 TB fits better describe the data.
- 2 TB features more evident at high bias (%R_n) and high Aspect Ratio (AR).

RESULTS: α, β, C's and g's

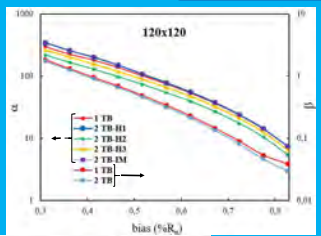

(1) β is independent of the 2 TB specific configuration. Its values using 1 TB and 2 TB differ slightly (few %).
(2) α depends on the 2 TB configuration, although it coincides for 2 TB-IM and 2 TB-H1 (algebraic result)
(H1: hypothesis $g_{TES,b} = g_{exp}$ (from IV's data))
α values change in some cases significantly. Bias dependence not strongly affected.

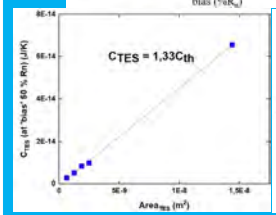

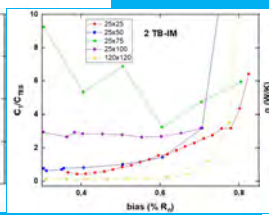

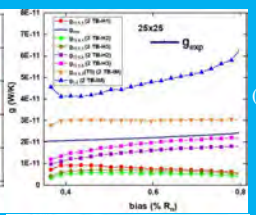

(1) C_{TES} (from one block):
- changes significantly (increases) when we use 2TB instead of 1TB.
- scales (increases proportionally) with TES size (area), with a scaling factor ~ 1,33C_{th} (*C_{th} is the calculated normal state heat capacity for the Mo/Au bilayer)*

(2) The extra heat capacity C_I in general can never be neglected ($C_I/C_{TES} \gtrsim 1$).

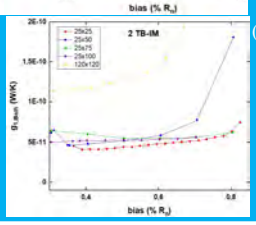

(1) All g's in all configurations display the same order of magnitude, thus emphasizing the need of considering 2TBs.
(2) The g's do not scale with TES perimeter; rather, there could be a g independent of TES size.

CONCLUSIONS

- The fitting procedures for Z(ω) using two thermal blocks have been developed.
- The impact of:
  (1) several fitting algorithms
  (2) initial values of fitting parameters

  on the fits quality and fitting parameters reliability have been evaluated.
- The relevance of the 2nd TB has been analyzed as a function of bias and TES size. It turns out that it is increasingly important as bias and TES aspect ratio increase.
- Two block configurations (hanging and intermediate) have been analyzed. The effects on TES parameters of these configurations and of their required hypotheses have been studied.
- The impact of the 2nd block on the logarithmic sensitivities α and β has been analyzed.
- TES thermal parameters (C's and g's) have been analyzed for the different configurations as a function of TES size; some preliminary conclusions have been drawn but more work is required to ascertain the suitable block configuration and identify the blocks.

REFERENCES

[1] K.D.Irwin and C.C. Hilton , "Transition-Edge Sensors in cryogenic particle detection". Topics in Applied Physics ed C Enss vol 99 (Berlin: Springer) (2005)
[2] J.N. Ullom, D.A. Bennett, "Review of superconducting transition-edge sensors for x-ray and gamma-ray spectroscopy", Supercond. Sci. Technol. 28, 084003 (2015)
[3] L. Fàbrega et al., "Towards Mo/Au based TES detectors for Athena/X-IFU", SPIE Proceed.Series 9144, 91445P (2014)
[4] I.J. Maasilta, "Complex impedance, responsivity and noise of transition-edge sensors: Analytical solutions for two- and three-block thermal models", AIP Adv. 2, 042110 (2012)

ACKNOWLEDGEMENTS

Financial support from the Spanish Ministerio de Ciencia e Innovación MICINN, through project RTI2018-096686-B-C22 and FPI contract (MM), is acknowledged. LF and MM acknowledge also MICINN for support through the Severo Ochoa Programme for Centres of Excellence (project FUNFUTURE, CEX2019-000917-S).

TAILORED SPIN-TEXTURES IN HYBRID SUPERCONDUCTING-FERROMAGNETIC STRUCTURES

A. Barrera, J. Alcalà , S. Martín , L. Balcells , M. Coll , N. Mestres , A. Palau

Institut de Ciència de Materials de Barcelona(iCMAB-CSIC), Campus UAB, 08193 (Barcelona) Spain.

INTRODUCTION

Superconducting cuprates mixed with ferromagnetic materials (FM-SC hybrids) present novel and unique electromagnetic tunability. Here, we show that by combining YBCO (SC) and permalloy (FM) materials in hybrid devices, one can manipulate magnetic textures, through loss-less superconducting stray fields or transport super-currents. Multiple magnetic states with different magnetoresistance signal can be stabilized at remanence and modified by applying small magnetic fields or currents . The proposed approach opens new venues for energy-efficient information storage and manipulation.

Hybrid SC-FM structures

The devices used in this study are composed of a YBCO (SC) strip perpendicular to a permalloy (FM) wire. Electrical measurements are based on magnetoresistance of permalloy by using four-point configuration and out-plane magnetic field.

a)

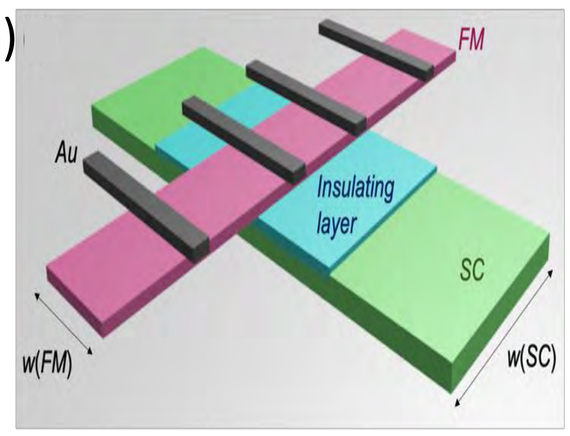

b)

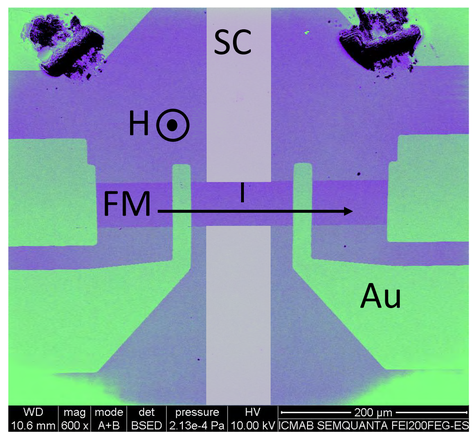

Anisotropic Magnetoresistance

Depending on the angle between permalloy magnetization and current direction, permalloy resistance changes. Magnetoresistance peaks obtained at the coercive field (maximum disorder of magnetic domain distribution).

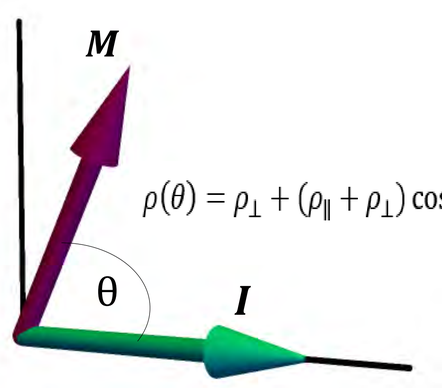

$$\rho(\theta) = \rho_{\perp} + (\rho_{\parallel} + \rho_{\perp})\cos\theta$$

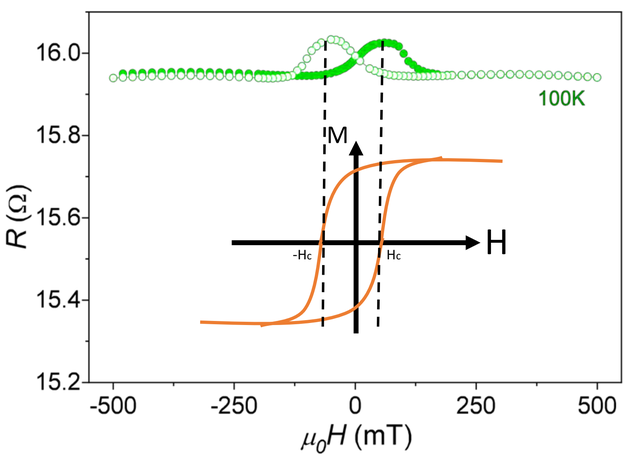

Effect of SC stray magnetic fields

Magnetic interaction between SC and FM materials is clearly observed in the magnetoresistance measurements .

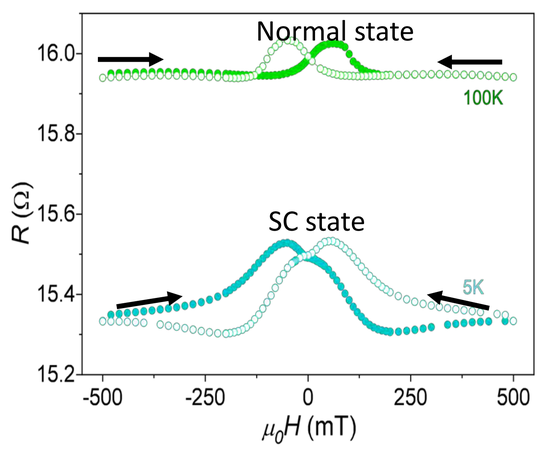

Peaks are shifted as a consequence to the coercive field variation.

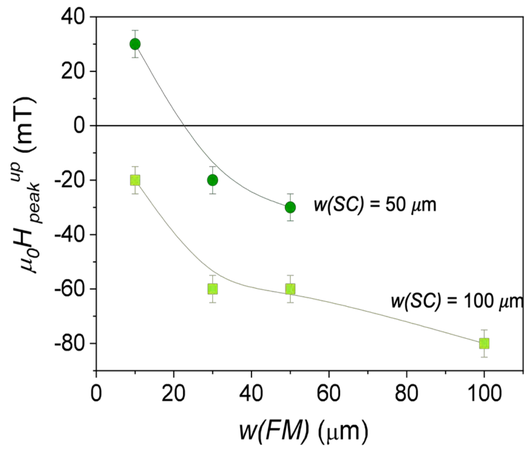

Peak shift enhanced for devices with wider SC and FM widths.

SC trapped magnetic fields

Magnetic states are stabilized at remanent state (0mT) depending on the maximum applied magnetic field .

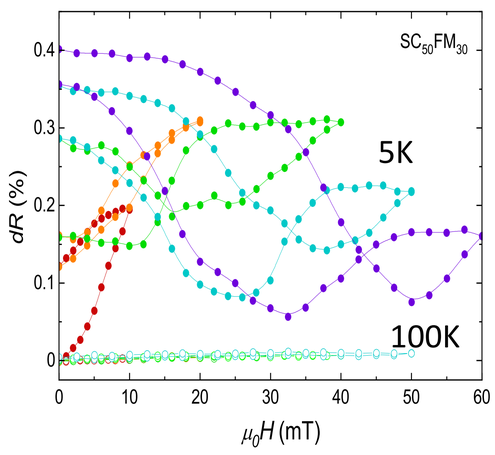

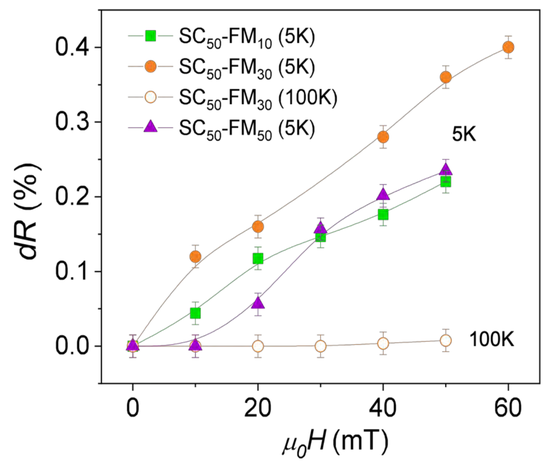

Multiple non-volatile magnetic states can be obtained depending on the device geometry or the applied magnetic.

Loss-free supercurrents

Injecting supercurrent through YBCO wire also generates a magnetic interaction with permalloy.

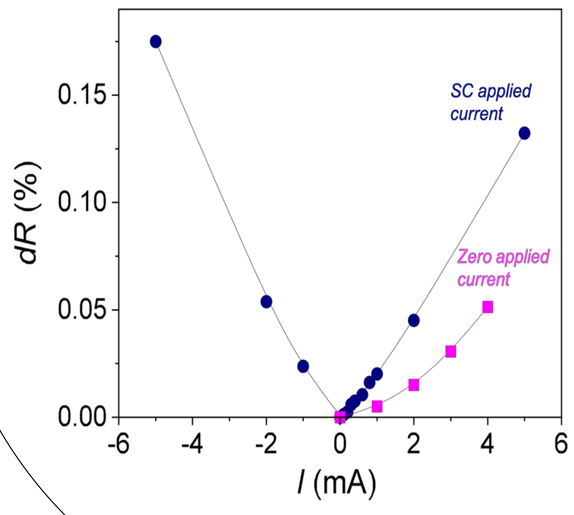

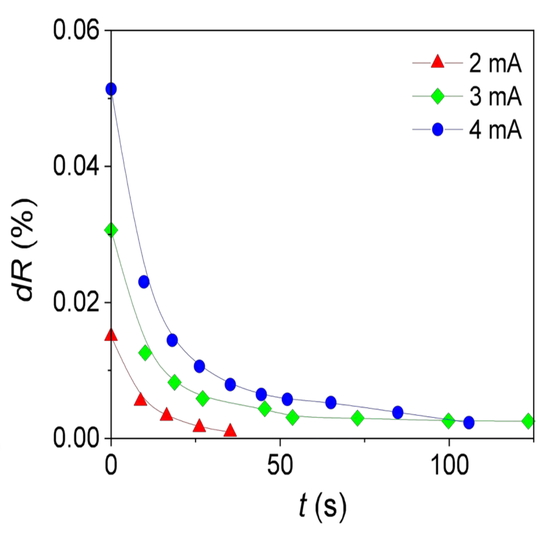

Multiple volatile magnetic states are obtained depending on the applied electrical current.

Conclusion

- Modulation of multiple magnetic states by combining FM/SC materials.
- Importance of geometry (SC and FM width) and the applied magnetic field o electrical current.
- Multiple and stable magnetic states can be achieved with magnetic field modulation.
- Loss-free supercurrents also allow to manipulate volatile magnetic states that decay in time.
- Application for different types of encoding and reading magnetic states.

REFERENCES

[1] J. Alcalà et al., Springer Nature Book, Chapt. 6. (2021)

ACKNOWLEDGEMENTS

We acknowledge financial support from Spanish Ministry of Science, Innovation and Universities (MICIU) through SUMATE project (RTI2018-095853-B-C21), co- financed by the European Regional Development Fund, and the METAMAG project (FUNMAT-FIP-2020), and Severo Ochoa FUNFUTURE (CEX2019-000917-S).We also thank support from the European Union for NANOCOHYBRI project (Cost Action CA 16218), and from the Catalan Government with 2017-SGR-1519 and Xarmae.

Determination of Chemical Oxygen Demand (COD) Using Nanoparticle-Modified Voltammetric Sensors and Electronic Tongue Principles

Grup de Sensors i Biosensors

Qing Wang, Manel del Valle*
Group of Sensors and Biosensors, Department of Chemistry,
Universitat Autònoma de Barcelona, 08193 Bellaterra, Barcelona, Spain
E-mail: manel.delvalle@uab.es

Universitat Autònoma de Barcelona

Abstract

This research focuses on the use of nanoparticle-modified voltammetric sensors for the rapid and green determination of Chemical Oxygen Demand in river waters and waters from agricultural waste. Four different variants of modified electrodes have been prepared: CuO nanoparticles electrogenerated over Cu and covered with Nafion film (CuO/Cu-Nf), and graphite–epoxy composites modified with Cu, CuO, and Cu–Ni alloy nanoparticles. The response features of these electrodes were assessed by calibrating them vs. glucose, glycine, ethylene glycol, and potassium hydrogen phthalate in alkaline media, as samples providing different difficulty in their (bio)degradation characteristics. The most sensitive electrode was demonstrated to be the (CuO/Cu-Nf) electrode, with an LOD of 12.3 mg $O_2 \cdot L^{-1}$. The joint information provided by the sensor array showed the ability of estimating both the organic load and the type of sample in terms of difficulty of degradation, in what can be named an intelligent sensor assembly.

Chemical Oxygen Demand (COD)

Chemical Oxygen Demand (COD) is defined as the amount of molecular oxygen (in milligrams of O_2) required to decompose all the organic compounds in 1 L of aqueous solution to carbon dioxide and water. There are many methods reported for COD determination, such as the conventional dichromate titration method. Electro-oxidizing the organic contaminants to completely transform them into CO_2 and H_2O using sensors is considered the best method for COD estimation [1-3].

Fabrication of Electrodes

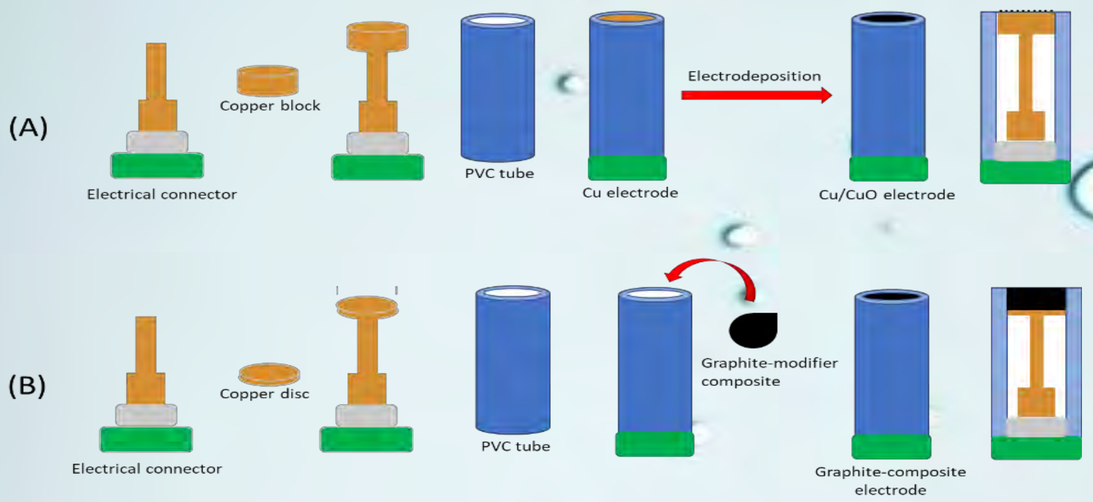

Figure 1. Diagram of the fabrication procedures of (A) the deposited Cu/CuO electrode and (B) the graphite–epoxy electrodes **(E2**, **E3** and **E4**) modified with metal nanoparticles (Cu, CuO and Ni Cu alloy, respectively)

Response Tests on Standard Compounds

1. Voltammetric Responses of Electrodes to Standard Compounds

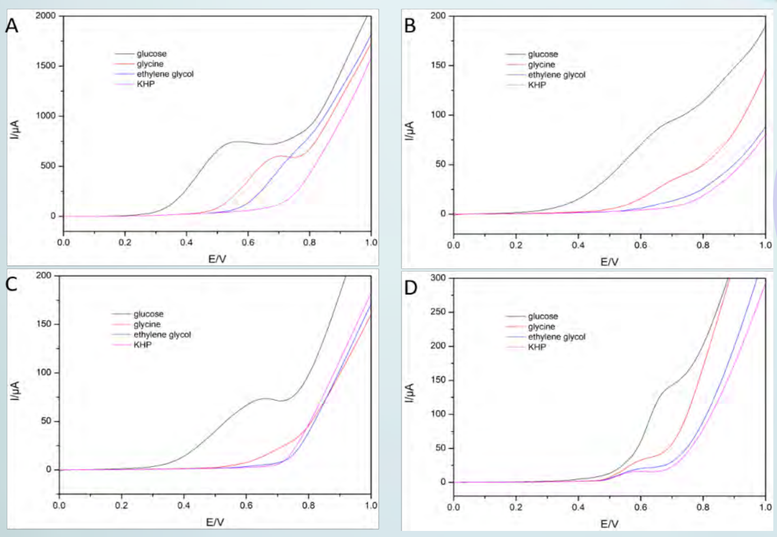

Figure 2. Oxidation curves of cyclic voltammetric responses of electrodes **E1** (A), **E2** (B), **E3** (C), and **E4** (D) to four standard chemical oxygen demand (COD) substances: 2.15 mM glucose; 2.15 mM glycine; 2.15 mM ethylene glycol; 2.15 mM KHP.

Different sensors show different cyclic voltammogram shapes and indicates the potential for distinguishing the main components and multivariate analysis

2. PCA on Standard Compounds

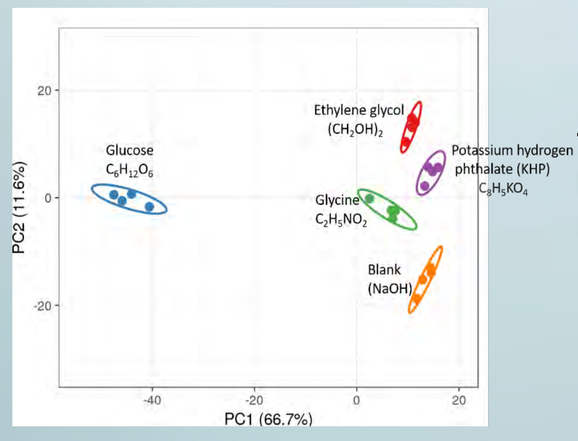

The level of degradation difficulty:
More easier, more left;
More difficult, more right.

Figure 3. Score plot of the first two components obtained after principal component analysis (PCA). A total of 20 samples were analyzed corresponding to quadruplicate determinations of glucose (blue), glycine (green), ethylene glycol (red), potassium hydrogen phthalate (purple), and blank (orange).

Real Samples Analysis

1. Calibration

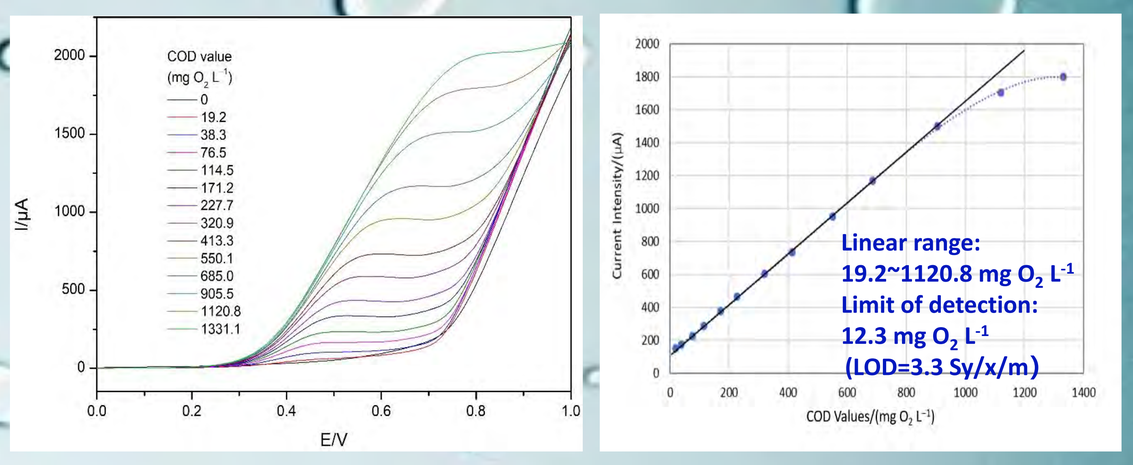

Figure 4. (A) Oxidation curves of cyclic voltammetric responses of electrode **E1** with the increase of addition of glucose in 0.05 M NaOH solution. (B) Calibration plot of intensity of current at E=0.7050 of electrode **E1** as a function of COD values (glucose as standard substance). Potential scan window, -1.0 to +0.7 V vs. Ag/AgCl (3.0 M KCl). Scan rate, 50 mV/s.

2. Spiking Tests

Table 1. Recovery yield of spiked glucose detected by electrode E1 towards Sample 1, 2 and 3.

	Sample found (mg O_2 L^{-1})	Added glucose (mg O_2 L^{-1})	Spiked sample found	Recovery yield (%)
Sample 1	<LOD	38.32	27.11	109.5
Sample 2	<LOD	38.32	27.67	108.6
Sample 1nd	33.76	95.52	112.11	82.02
Sample 2nd	17.10	95.52	101.64	88.51
Sample 3nd	18.56	95.52	97.37	82.50

nd Spiking tests of real samples with fewer dilution.

3. PCA on Real Samples and Standard Compounds

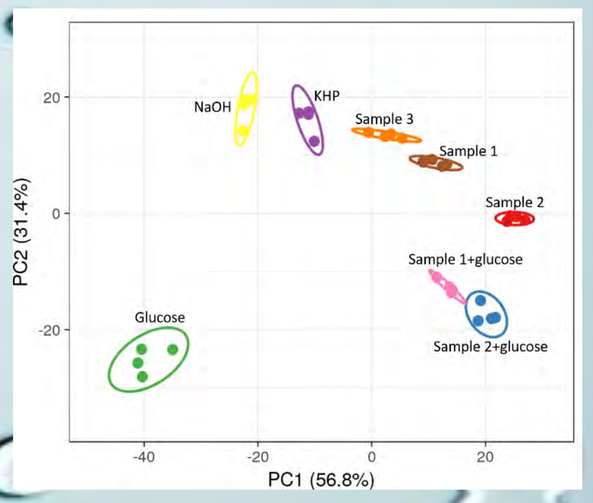

Sample 2, which contains lots of pesticides, is on the right. Sample 1 contains fewer pesticides than Sample 2, more left. Sample 3 also contains some organic compounds that are difficult to be degraded.

Figure 5. Score plot of the first two components obtained after PCA analysis to real samples and standard substances. These samples are glucose (green), NaOH (yellow), potassium hydrogen phthalate (purple), Sample 1 (brown) and its spike with glucose (pink), Sample 2 (red) and its spike with glucose (blue), and Sample 3

Conclusion

This work developed an easy method of analyzing wastewaters quantitatively and qualitatively by combining the electrochemical electrodes with the electronic tongue technique. The COD values were calculated based on the calibration and the PCA technique can be used to evaluate the main component of a river sample, which is easy or difficult to be degraded. The resulting sensor-based method demonstrates great potential not only for estimating the precise value of organic load but for predicting the difficulty behavior in its degradation.

Acknowledgements

Financial support for this work was provided by Spanish Ministry of Science and Innovation trough the project CTQ 2016-80170 and by program ICREA Academia from Generalitat de Catalunya. Qing Wang thanks the support of Universitat Autònoma de Barcelona and China Scholarship Council for the UAB-CSC joint scholarship.

icrea Institució Catalana de Recerca i Estudis Avançats

China Scholarship Council

Ministerio de Economía y Competitividad

References

[1] C. R. Silva, C. D. C. Conceiçao et al., *J Solid State Electrochem*, **2009** (13), 665-660;
[2] T. Carchi, B. Lapo and L. Fernéndez et al., *Sensors*, **2019** (19), 669-685.
[3] M. Gutiérrez-Capitán,A. Baldi et al., *Anal. Chem.* **2015**, 87, 2152–2160

Tuning the electronic structure of High Temperature Superconducting films by field-induced oxygen diffusion

Contact:
jalcala@icmab.es

J. Alcalà[1], A. Fernández-Rodríguez[1], S. Marinkovic[2], S. Collienne[2], S. Blanco Alvarez[2], S. Melinte[2], X. Granados[1], N. Mestres[1], A. V. Silhanek[2], A. Palau[1]

[1] Institut de Ciència de Materials de Barcelona, ICMAB-CSIC, Campus UAB, Bellaterra (Barcelona), Spain
[2] Experimental Physics of Nanostructured Materials, Q-MAT, CESAM, Université de Liège, B-4000 Liège, Belgium

Motivation

Modulation of carrier concentration in strongly correlated oxides offers the unique opportunity to induce different phases in the same material, which dramatically change their physical properties. Specially, the possibility to reversibly modify the metal-insulator transition (MIT) in perovskite oxides, by means of an electric field, as the external control parameter, is a very active area of research in condensed matter physics, and a promising technique to generate new solid-state devices with exciting functionalities. In this contribution we will show the electric manipulation of the superconducting to insulator phase transition (SIT) in high temperature superconductor $YBa_2Cu_3O_{7-\delta}$ films by field-induced oxygen doping. We demonstrate that non-volatile volume phase transitions can be locally modulated to generate transistor-like devices, with free-resistance channels, in which the electric field magnitude and direction, temperature, and anisotropic oxygen mobility determine their characteristics.

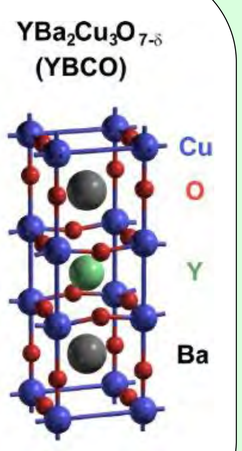

Phase diagram of strongly correlated cuprates and multilevel states

- **Field Induced MIT / SIT:** Non volatile Reversible Metal (Superconductor) - Insulator transitions through an optimal modulation of their carrier concentration.

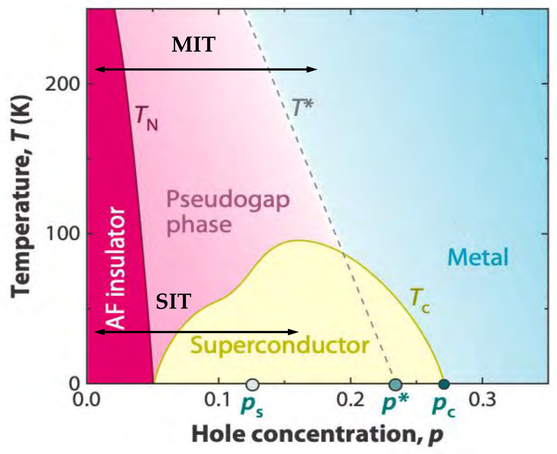

*Taillefer , **Annu. Rev. Condens. Matter Phys**. 1, 51–70 (2010)*

- Field-induced reversible robust volume Metallic to Insulator Transition (MIT) through oxygen doping:

→ Fabrication of gate-tuneable transistor-like devices (operating at RT or below T_c)

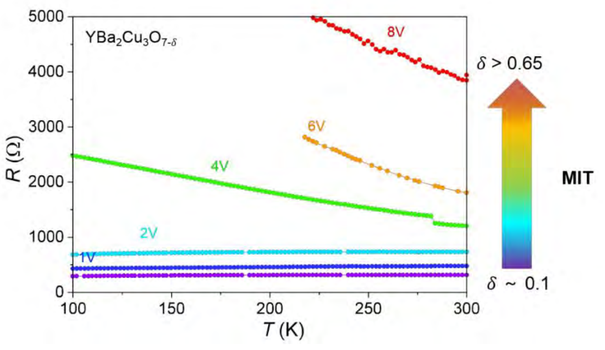

*Palau et al. **ACS Mat. & Interf.** 10, 30522 (2018), Fernandez-Rodriguez et al. **Materials** 13, 281 (2020)*

High temperature MIT

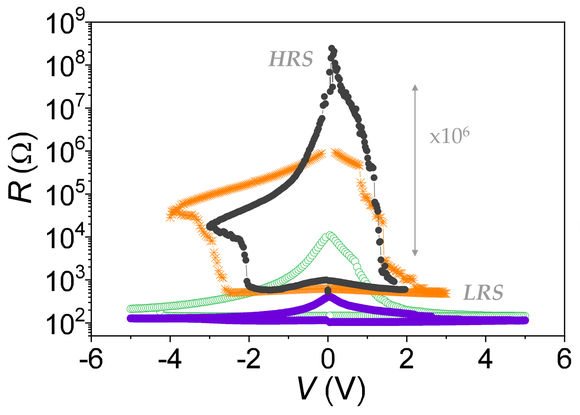

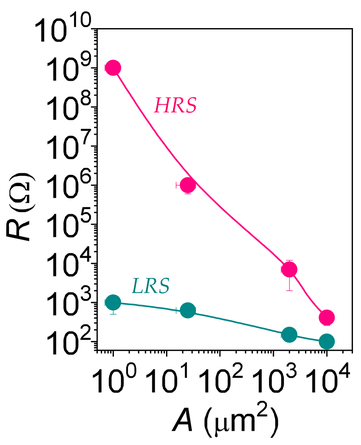

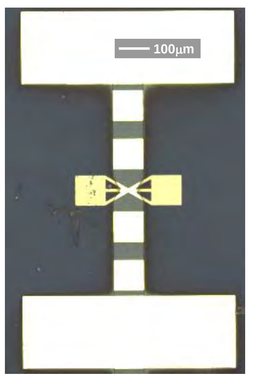

- **Area dependent resistance values** consistent with a switching effect homogeneously distributed underneath the electrode.
- Very large switching ratios obtained with moderate low V pulses by using micrometric contacts.

Switching Superconducting parameters

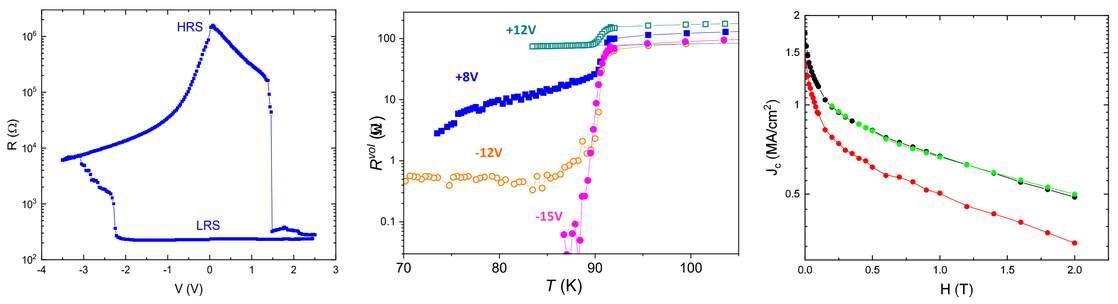

- **Ionic carriers move anisotropically**, creating a lateral oxygen diffusion of hundreds of microns away from the contacts.
- Locally modulate the superconducting order parameter by using a micrometric contacts → reconfigurable pinning potentials
- Reversible changes in the J_c(H) dependence → reconfigurable pinning landscape

Direct visualization of current induced O migration

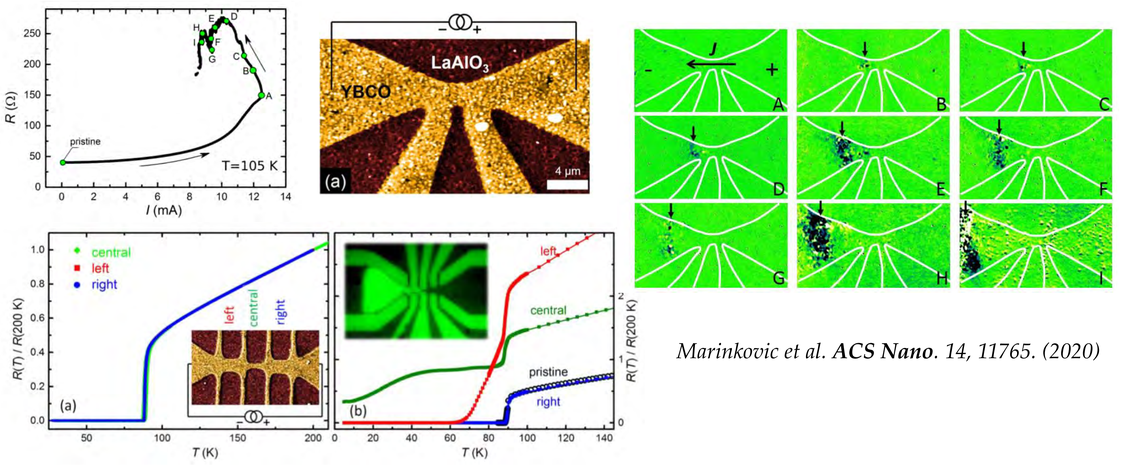

*Marinkovic et al. **ACS Nano**. 14, 11765. (2020)*

- Area with oxygen vacancies clearly visible as a bright region in microscope images. Clear modulation of Tc (hence oxygen doping) at different regions of the YBCO constriction.
- Tuning the oxygen content by current induced oxygen migration in YBCO thin films (Electromigration).
- Oxygen vacancy displacement towards the cathode (−) visible by optical microscopy.

Conclusions

We have shown the resistive switching in metallic oxide perovskites that corresponds to a field-induced modulation of the carrier concentration. Volumic robust effect with High R ratios and also multilevel, reversible and non-volatile states with long retention times. Experimental evidence through Hall measurements, micro-Raman, and optical microscopy that the electromigration process allows a selective displacement of oxygen atoms. Powerful alternative to locally fine-tune the charge carrier density in cuprates and study of the phases appearing in their doping phase diagram.

Acknowledgments: Spanish Ministry of Science and Innovation through Severo Ochoa FUNFUTURE (CEX2019-000917-S) and SUMATE (RTI2018-095853-B-C21) projects, co-financed by the European Regional Development Fund and the METAMAG project (FUNMAT-FIP-2019). European Union for NanoSC Cost Action NANOCOHYBRI (CA16218), the Catalan Government with 2017-SGR-1519 and XARMAE.

ICMAB INSTITUT DE CIÈNCIA DE MATERIALS DE BARCELONA · EXCELENCIA SEVERO OCHOA · CSIC · UAB Universitat Autònoma de Barcelona · Generalitat de Catalunya · GOBIERNO DE ESPAÑA · MINISTERIO DE CIENCIA E INNOVACIÓN

High throughput fabrication of Single Electron Devices based on Silicon Nanowires with embedded Quantum Dot

D. Bricio-Blázquez[1], A. Kapas[1,2], A. Guerrero [1], J. Sánchez [1], A. García[1], R. Mas [1], X. Borrisé[3], J. Bausells[1], F. Perez-Murano[1] and J. Llobet[1]
[1]Institute of Microelectronics of Barcelona (IMB-CNM CSIC), Bellaterra, Catalonia, E-08193, Spain
[2]Universitat Autónoma de Barcelona (UAB), Bellaterra, Catalonia, E-08193, Spain
[3]Catalan Institute of Nanoscience and Nanotechnology (ICN2), CSIC and The BIST, Bellaterra, 08193, Catalonia, Spain
e-mail: David.Bricio@imb-cnm.csic.es

Abstract

We are developing a high throughput fabrication process of single-electron devices (SED). The SED is base in on silicon nanowire (SiNW) in which a quantum dot (QD) will be generated.

The main features are:
- High accuracy and dimensional control
- Mix-and-match approach based on optical an electron beam lithography (EBL) with 5 lithographic levels.
- Placement of a QD in a SiNW by means of ion implantation.

Keywords: ***SED, Quantum Dot, Nanowire, Mix-And-Match approach***

Objectives

- Produce a reliable SiNW platform to experiment novel nanofabrication process of SED.
- Fabrication at wafer scale.
- Placement of the QD in the middle of the SiNW.
- Ultimately achieve deterministic single doping.

Fabrication process

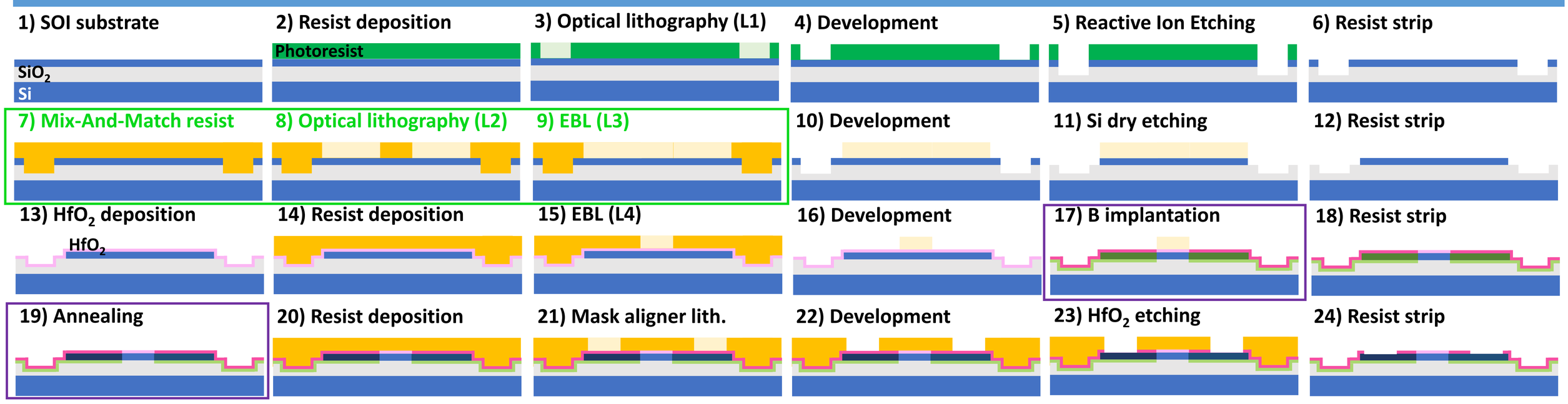

Results

Mix-And-Match

Height of the resist after lithography

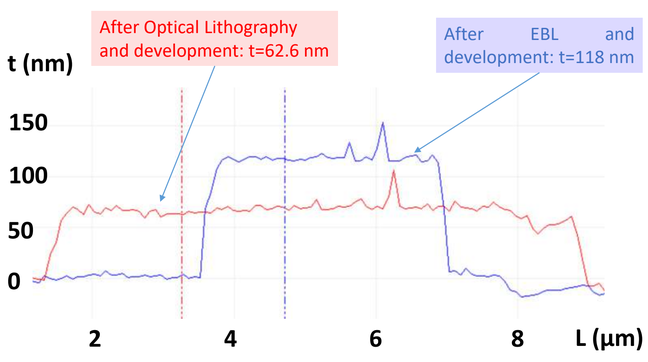

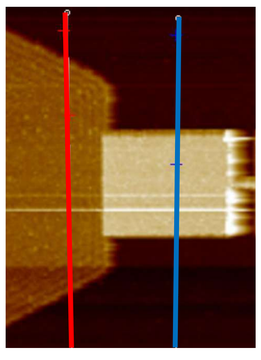

Dimensional characterization

Proximity effect due to the EBL exposure

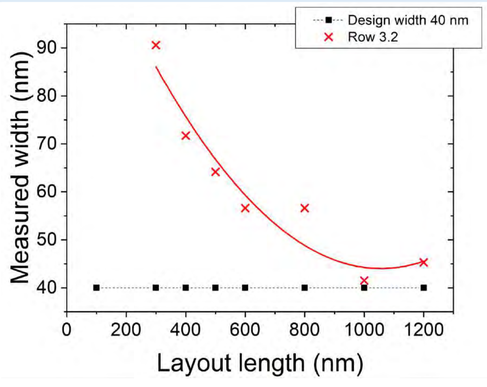

Length of the SiNWs

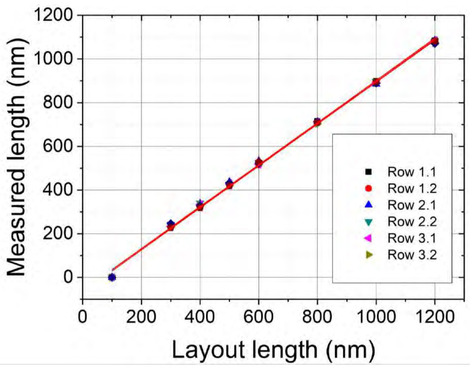

Uniformity analysis

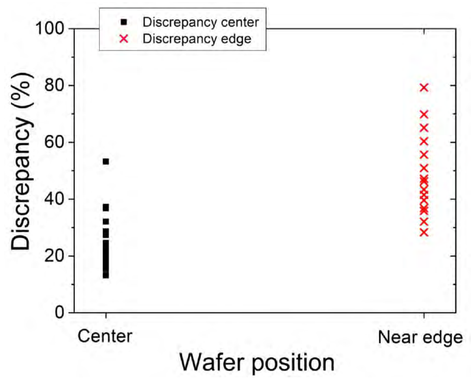

SEM characterization

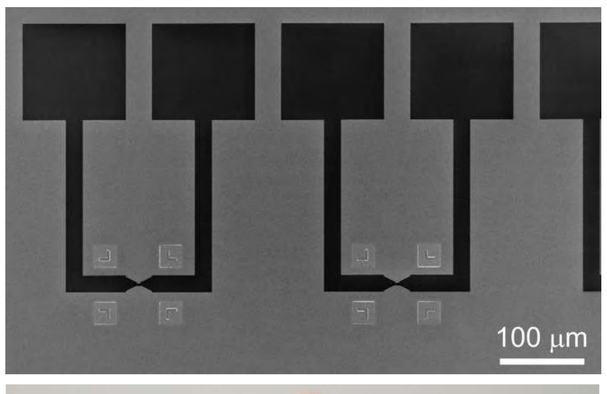

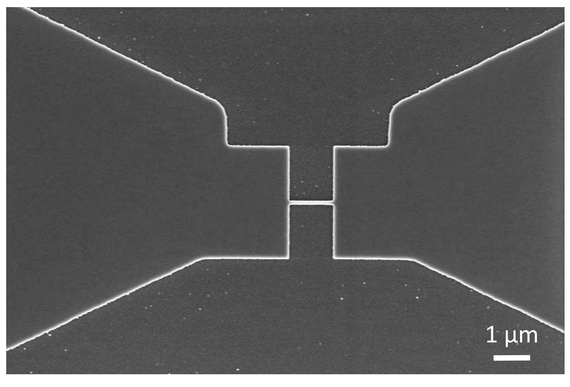

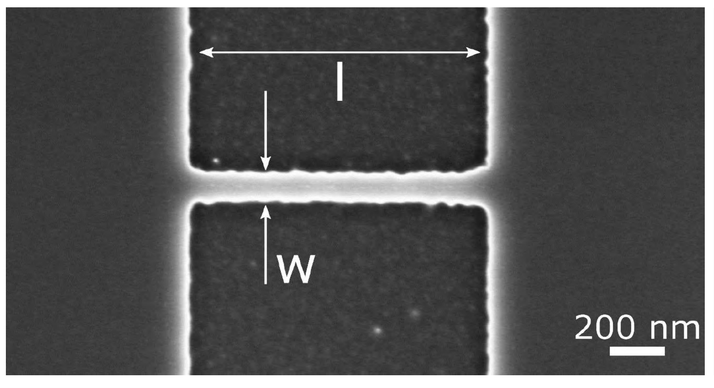

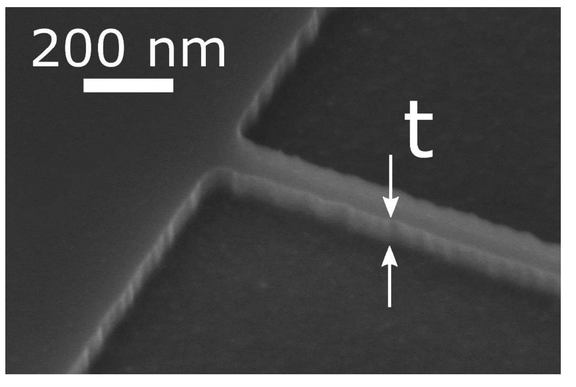

Conclusions

- Mix-and-match resist has been tuned properly.
- The alignment marks allow an appropriate alignment among the lithographic levels.
- The correlation between the layout width and the real one of the SiNWs improves as the length increases (Proximity effect is reduced).
- High throughput fabrication at wafer level has been demonstrated, getting more than 5000 individually connected SiNWs, with higher dimensional accuracy at the center of the wafer compared with the edge.

Future work

- Continuing the process at full wafer.
- Tuning the process to reach higher agreement between the layout dimensions and the real dimensions of the nanowires.
- To improve the smoothness of nanowires.
- Continue the development of a method to place a QD in the middle of the SNW in a deterministic manner.

Acknowledgements

Special thanks to our IMB-CNM CR engineers colleagues and the funding agencies:
NEP (Horizon 2020) – Nanoscience Foundries and Fine Analysis;
STARSED Project (national funding); SiM-SeT Project (MSCA)

Founded by the European Union and the Generalitat de Catalunya under the Beatriu de Pinós program (COFUND 801370 for Marie-Skłodowska-Curie)

Exploring the implications of ligno-suberin barriers and related metabolites for resistance against bacterial wilt in tomato

Álvaro Luis Jiménez-Jiménez[1], Anurag Kashyap[1,2], Montserrat Capellades[1,3], Weiqi Zhang[1] , Sumithra Srinivasan[4], Anna Laromaine[4], Olga Serra[5], Mercè Figueras[5], Jorge Rencoret[6], Ana Gutiérrez[6], Marc Valls[1,7], Nuria S. Coll[1,3]

1 Centre for Research in Agricultural Genomics (CRAG), CSIC-IRTA-UAB-UB, Campus UAB, Bellaterra, Spain

2 Department of Plant Pathology, Assam Agricultural University, Jorhat, Assam 785013, India

3 Consejo Superior de Investigaciones Científicas (CSIC), Barcelona, Spain, 4 Institute of Material Science of Barcelona (ICMAB), CSIC, Campus UAB, Bellaterra, Spain

5 Laboratori del Suro, Biology Department, Universitat de Girona, Campus Montilivi, Girona, Spain, 6 Institute of Natural Resources and Agrobiology of Seville (IRNAS), CSIC, Seville, Spain

7 Department of Genetics, Universitat de Barcelona, Barcelona, Spain

alvaro.jimenez@cragenomica.es

Background

The soil borne pathogen *Ralstonia solanacearum* is the causative agent of bacterial wilt, a devastating disease for major crops of agronomic interest. This bacterium enters the plants through wounding points at the roots, reaching the vasculature, where it proliferates massively in the xylem, provoking rapid wilting.

We characterized a specific feature of the highly resistant tomato cultivar Hawaii 7996 (H7996): the deposition of ligno-suberin barriers and related metabolites such as hydroxycinnamic acid amides (HCAAs) upon infection with *Ralstonia* at the root vasculature, resulting in a physical restriction of pathogen colonization throughout the plant.

To further study the contributions of these physico-chemical barriers to disease resistance, we analyzed transgenic tomato lines overexpressing genes from the ligno-suberin pathway that were significantly resistant to infection, finding structural changes in the root xylem vasculature consistent with reinforced cell walls that help blocking intruder invasion.

Resistant H7996 tomato restricts R. solanacearum colonization and induces a vascular coating response

(a) Resistance phenotype in H7996. (b) Increase in H7996 wall-bound autofluorescence when challenged with R.solanacearum infection. (c) H7996 increase in autofluorescence non-quenched by Phloroglucinol staining, normally attributed to the phenolic fraction of suberin barriers, and a lignin polymer resistant to pathogen attack, in contrast to susceptible Marmande plants.

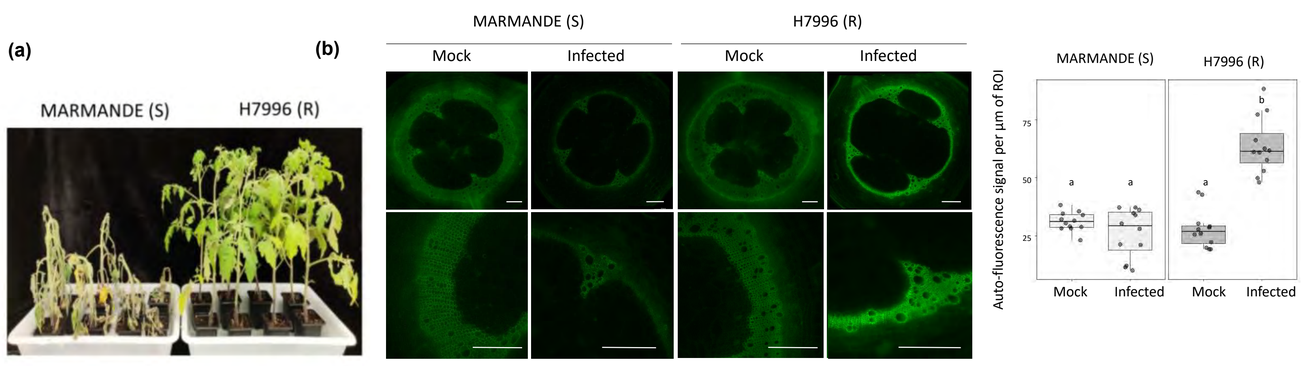

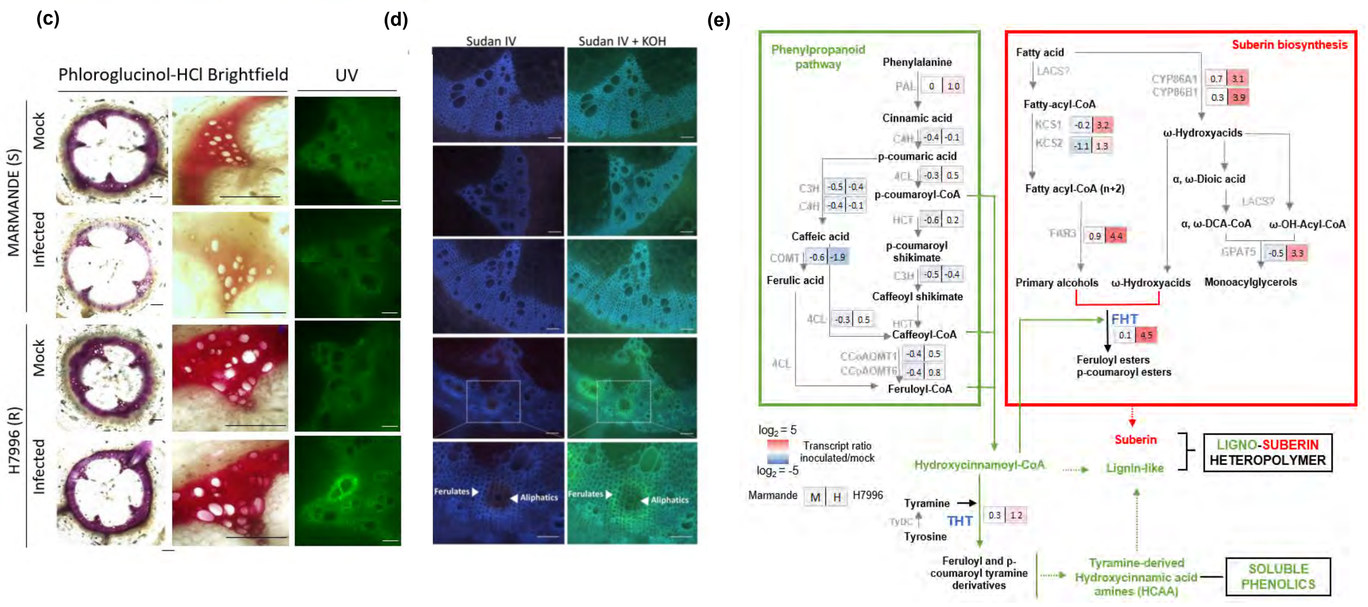

(d) Production of suberin aliphatics in H7996 vasculature, shown as brownish areas with Sudan IV staining, and ferulate/feruloylamide deposits as a blue-to-green conversion of autofluorescence upon alkali treatment. (e) Transcriptional analysis by qRT-PCR confirmed a significant upregulation of genes coding for the ligno-suberin pathway in H7996 upon infection.

Conclusions

H7996 responds to R.solanacearum infection with deposition of ligno-suberin barriers and HCAAs at the root xylem vasculature

Overexpressing genes from this metabolic pathway in susceptible tomato backgrounds revealed that the production of HCAAs in SlTHT1-3 confers resistance against *R. solanacearum.*

Based on this data, we propose that these induced barriers do not only restrict pathogen colonization, but also confer antimicrobial properties to the cell walls, showing this pathway as a promising source of resistance against this devastating disease in tomato.

Methodology

Thin cross-sections were made out of *R.solanacearum*-infected or mock-treated plants, in the transition between the basal hypocotyl and the taproot, below the soil line. Sections were kept in 70 % ethanol at room temperature for 5-7 days to remove chlorophyll. Phloroglucinol-HCl stain was used for lignin detection under brightfield observation, and Sudan IV for detecting suberin aliphatics under UV light. An alkali treatment with 1N KOH (pH=10) was also performed to detect wall-bound ferulates as a blue-to-green autofluorescence conversion in the mounted cross-sections.

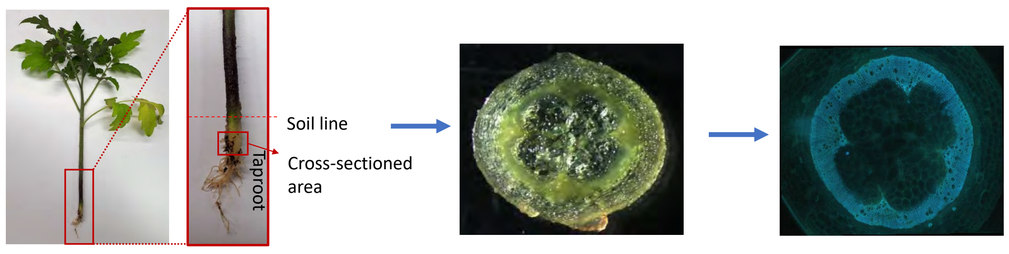

Overexpression of SlTHT1-3 in a susceptible tomato cultivar confers resistance to R. solanacearum

Genes involved in ferulate esterification into suberin aliphatics and feruloylamide synthesis, such as SlFHT and SlTHT1-3, respectively, were overexpressed in suscetible tomato, since these genes were also upregulated in H7996 upon infection. (a) SlFHT showed a slight delay in disease progression, (b) while the THT line was highly resistant to the disease.

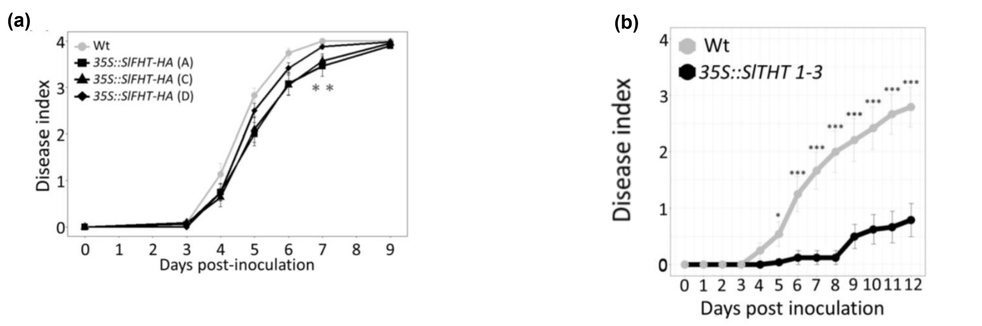

SlTHT1-3 histological studies showing structural changes in ligno-suberin barriers: (a,d) increase in autofluorescence non quenched by phloroglucinol, presence of ferulate deposits upon KOH treatment, with no suberin aliphatic fractions (b,c,e).

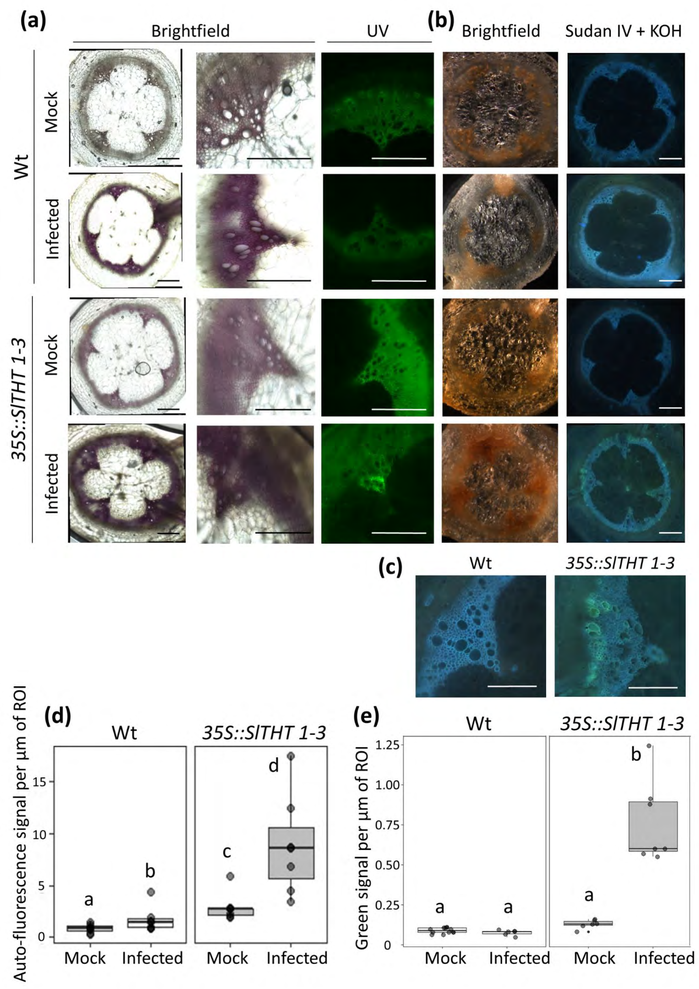

References

Kashyap, Anurag, et al. "Induced ligno-suberin vascular coating and tyramine-derived hydroxycinnamic acid amides restrict Ralstonia solanacearum colonization in resistant tomato roots." *bioRxiv* (2021).

Dramatic drop in cell resistance through induced dipoles and bipolar electrochemistry.

L. Fuentes-Rodríguez [1,2], Ll. Abad[2], E. Pujades-Otero[1], P. Gómez-Romero[3], D. Tonti[1], N. Casañ-Pastor*[1]

[1] Institut de Ciència de Materials de Barcelona-CSIC, [2] Institut de Microelectrònica de Barcelona-CNM-CSIC, [3]Catalan Institute of Nanoscience and Nanotechnology, ICN2 (CSIC-BIST)

Campus UAB, 08193 Bellaterra, Barcelona, Spain

l.fuentes@icsic.es

SUMMARY

When conducting materials are immersed in an electrolyte, induced dipoles and bipolar electrochemistry processes change the electrochemical cell characteristics. Simple polarization effects or electric percolation had not been sufficient to explain those changes in suspensions, since those changes occur well below the electronic percolation limits. This work shows that a significant lower resistance of the cell and charge transfer effects are present even for a discrete number of non-mobile conducting pieces inserted unconnected in the blank electrolyte. Using macroscopic conducting immersed pieces, a physical mediation due to transport through the induced dipoles is observed and if redox species exist, is enhanced. The combination is considered a physicochemical mediation.

Induced Dipole evaluation for immersed conducting pieces.

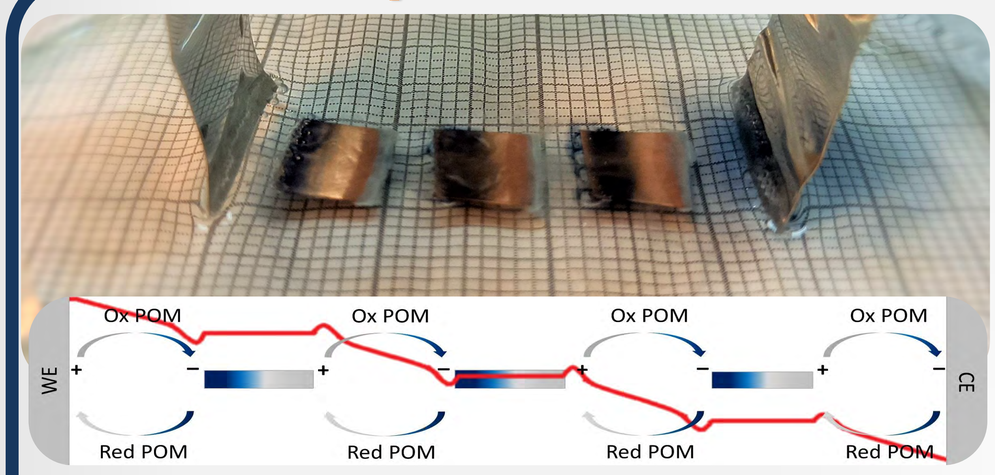

Figure 1. *Image and scheme of redox mediation between existing induced dipoles.*

An induced dipole is created between the borders of each of the conducting pieces in the electrolyte, when an external electric field is applied.

The existence of such dipole and the voltage contribution may be established by various semi-quantitative approaches.

$SiW_{12}O_{40}^{-4}$ *(colorless)* ***+2e- → $SiW_{12}O_{40}^{-6}$ (dark blue)***

(induced cathode)

And reoxidation at induced anode.

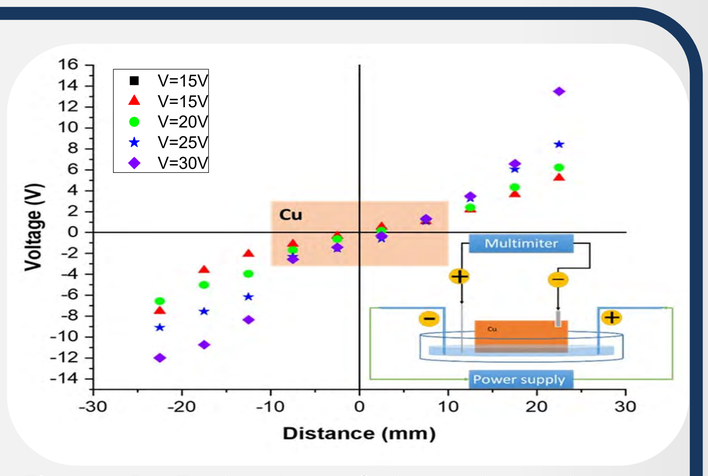

Figure 2. *Evaluation of the voltage between poles.* ***The induced voltage between the copper poles is about 1/10 of the applied external voltage.***

Resistivity changes for electrolyte containing immersed conducting pieces (EIS)

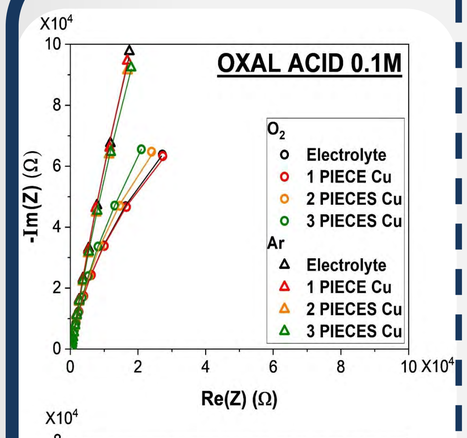

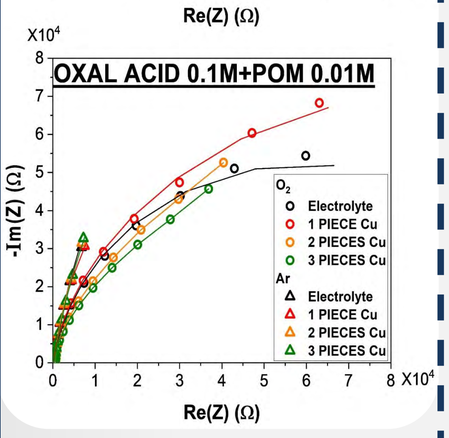

Figure 4. *Nyquist plot*

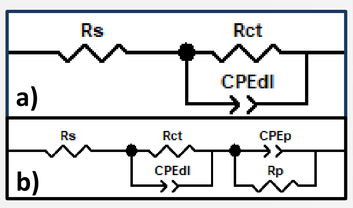

Figure 3. *Equivalent circuit a) for electrolyte b) including immersed conducting pieces.*

Elements:

R_s → *Resistance of solution*

CPE_{dl} → *Constant phase element of the double layer*

R_{ct} → *Resistance of the charge transfer*

CPE_p → *Constant phase element of the double layer of the pieces immersed*

R_p → *Resistance of polarization pieces immersed.*

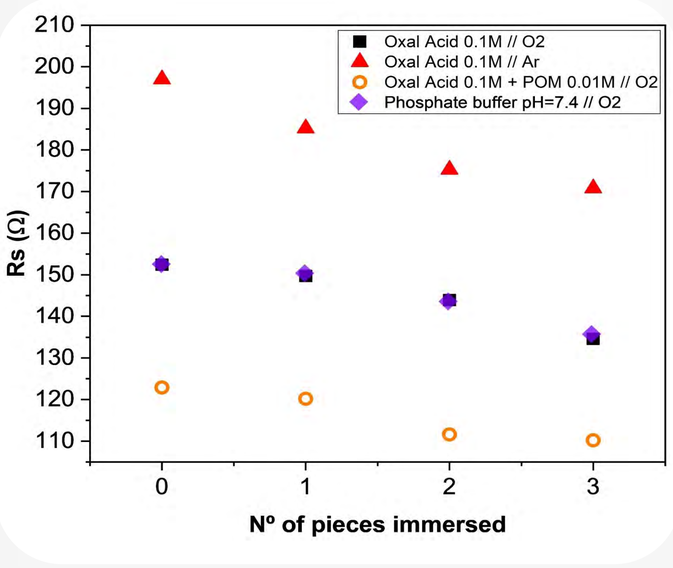

Figure 5. *Rs for solutions containing 0,1,2,3 Cu pieces.*

The resistance is dramatically decreased in an electrochemical cell when immersing discrete conducting pieces in the electrolyte.

The effect depends on the number of pieces, its size and shape, as well as the location within the electric field.

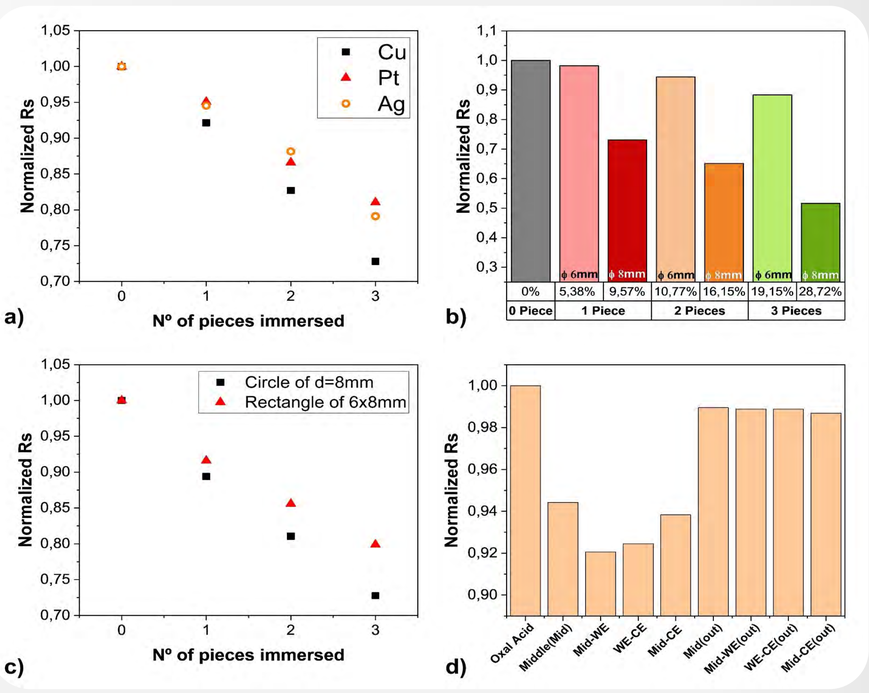

Figure 6. *Relative Rs changes for oxalic acid solutions (O2) immersing circular pieces.*

Cyclic voltammetry changes for redox species (POM)

If we choose the redox behavior of $SiW_{12}O_{40}^{-4}$ (POM) anion, we do observe some changes.

Figure 7. CV

E_{max}: *reduction shift to lower absolute values for more pieces added.*

I_{max}: *intensity reduction and oxidation waves is also increased.*

Poles of opposite signs from different pieces are facing each other, any species that has a redox process may act as a mediator.

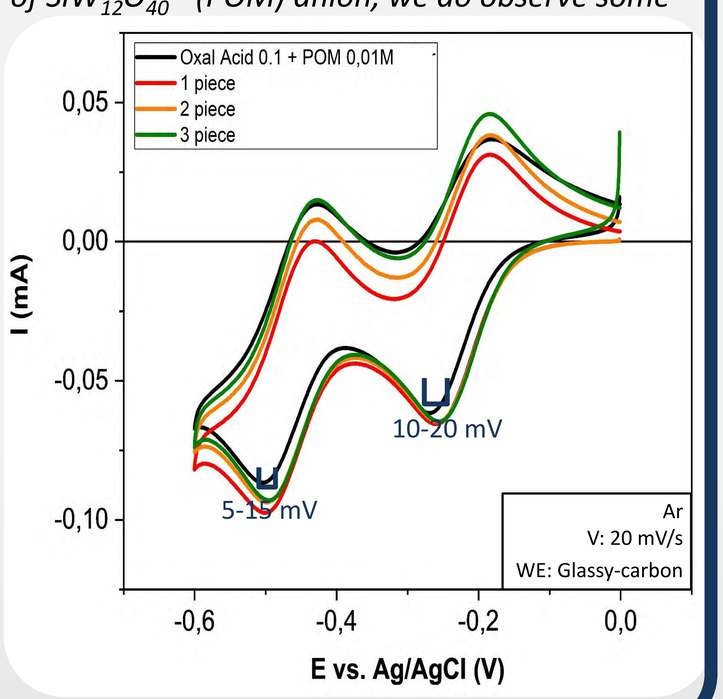

CONCLUSIONS

- ✓ ***The R_s decreased when immersing discrete conducting pieces in the electrolyte, even without electronic percolation.***
- ✓ ***The R_s effect depends on the number of pieces, its size and shape, as well as the location within the electric field.***
- ✓ ***Physical polarization effects appear but also modifications in redox potentials, and capacitive effects, much before electronic percolation exists.***
- ✓ ***Physical mediation, seen as a cascade effect, is envisaged through the formation of alternating dipoles, while chemical mediation exists at the new induced interfaces.***

Acknowledgements

Ministery of Science of Spain through grants RTI2018-097753-B-I00, CEX2019-000917-S and RYC-2013-12640

References

Dramatic drop in cell resistance through induced dipoles and bipolar electrochemistry. *L. Fuentes-Rodríguez , Ll. Abad, E. Pujades, P. Gómez-Romero, D. Tonti, N. Casañ-Pastor*. J.Electrochem.Soc. 2021 – Under revision

Silicon Nanowire Single Hole Transistor with Boron Quantum Dot Fabricated by Electron Beam and Focused Ion Beam Lithography Technologies.

A. Kapas [1,2], D. Bricio-Blázquez[1], M. Duch[1], A. García[1], A. Guerrero[1], J. Bausells.[1] ,X. Borrisé[3], F. Perez-Murano[1], J. Llobet[1].
[1]. Institute of Microelectronics of Barcelona (IMB-CNM CSIC), Bellaterra, Catalonia, E-08193, Spain
[2]. Universitat Autónoma de Barcelona (UAB), Bellaterra, Catalonia, E-08193, Spain
[3]. Catalan Institute of Nanoscience and Nanotechnology (ICN2), CSIC and The BIST, Bellaterra, 08193, Catalonia, Spain

ABSTRACT

Single-hole transistors have been identified as promising semiconductor devices for quantum computation. The fabrication of miniaturised nanoelectronics based on silicon sub-10 nm gate is still challenging and opens the possibility to build quantum devices.

In previous works we demonstrated the single-charge effect characteristics in the I/V curves at low temperature in similar devices [1,2]. In this work we designed single-hole transistors made of p-type silicon nanowires, which incorporates doped silicon quantum dots. The transistor fabrication method uses rapid, high resolution, scalable and reproducible processes, based on electron beam and focused gallium ion beam lithography techniques, ion implantation, anisotropic wet etching, and thermal processes.

CHALLENGES

- Boron doping characterization after the diffusion process.
- Control the boron doping diffusion in the middle of the SiNW to get a QD.
- Integrate the device as a scallable methodology

MATERIAL Modeling and Characterization

Boron diffusion simulation

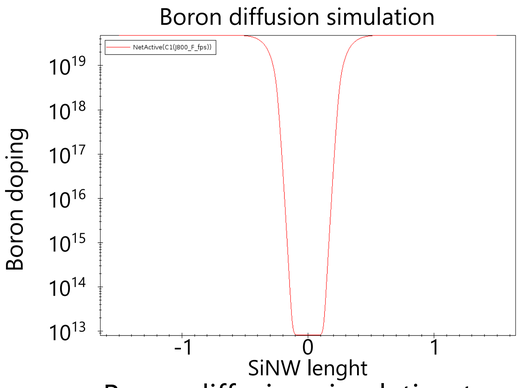

Boron diffusion simulation to achieve a few atoms of boron in the middle of the SiNW.

Silicon Raman Spectra

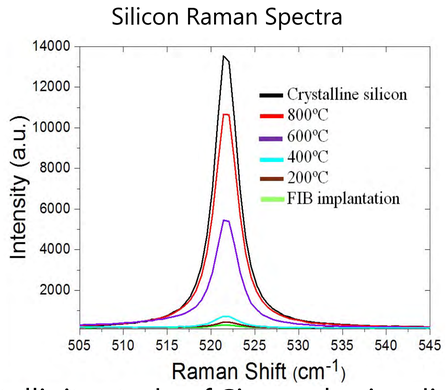

Crystallinity study of Si samples irradiated with Ga after different temperature annealing.

Boron implantation

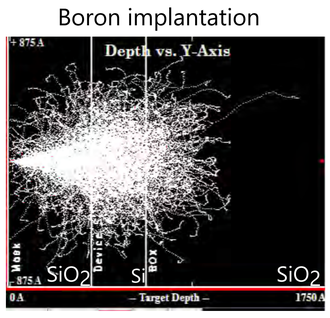

Montecarlo simulations to study ion implantation across the layers.

Gallium out-diffusion

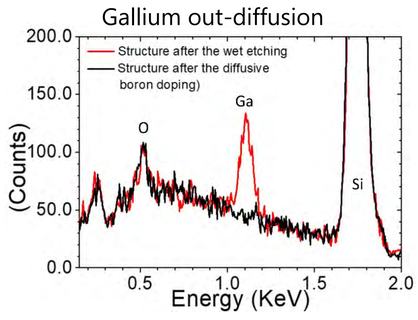

EDX analysis before and after the thermal annealing. It is seen the out-diffusion of Ga after annealing process.

RESULTS

I/V SiNW characterization

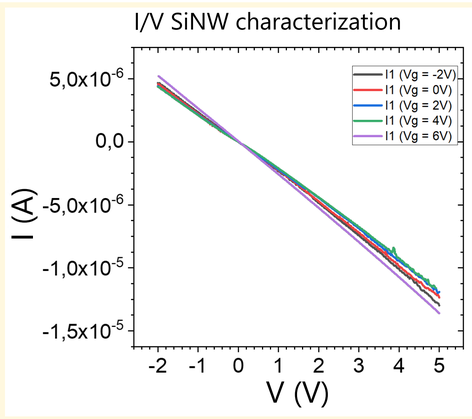

Measurement of the electrical resistance of the SiNW for different gate voltages at room temperature.

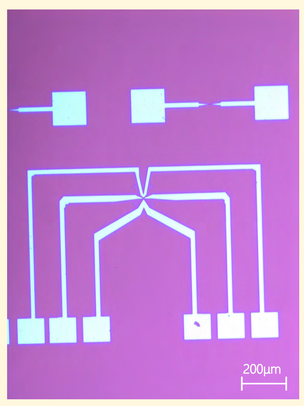

Optical microscope image of the final device

FABRICATION APPROACH

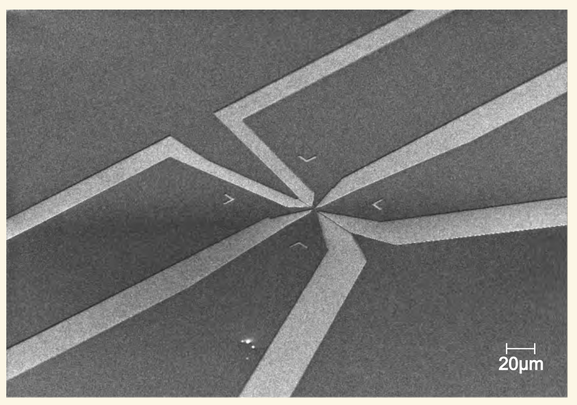

Top-view SEM image showing the lithographic alignment marks and the lines that connect the SiNW. These areas where boron is implanted.

1

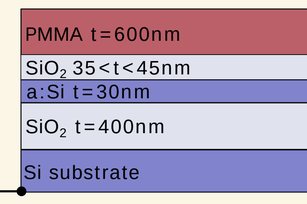

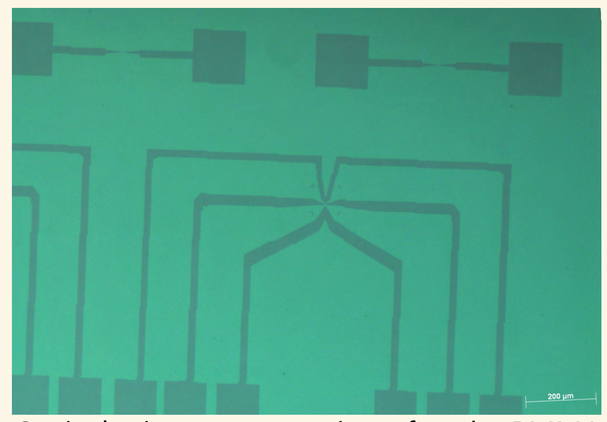

Optical microcopy top-view after the PMMA developement.

2

PMMA exposition by EBL

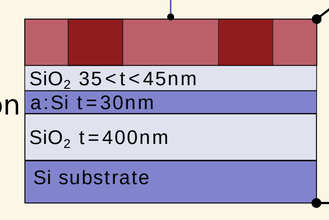

3

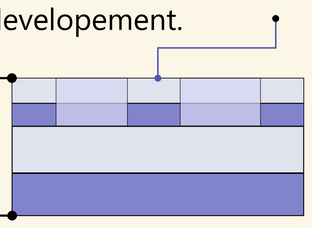

- PMMA development
- Boron implantation
- PMMA strip

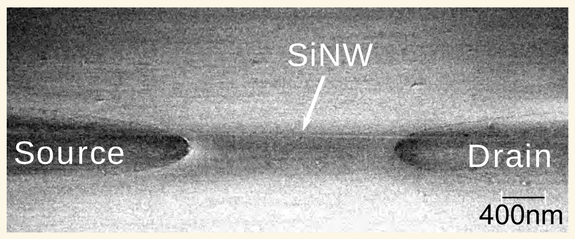

Top-view SEM image of SiNW and contacting pads after FIB implantation.

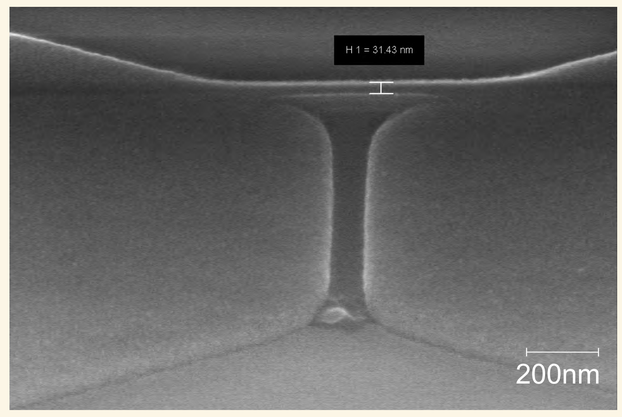

Contacting pads and SiNW after wet etching. It is observed a 30nm thick SiNW.

FIB implantation

4

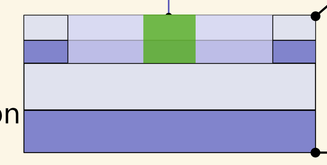

5

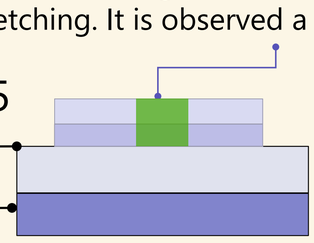

- SiO_2 wet etching
- TMAH wet etching

6

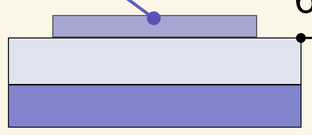

Thermal annealling

SPECIAL ACKNOLEDGEMENT

Special thanks to our IMB-CNM CR engineers colleagues and the funding agencies:
NEP (Horizon 2020) – Nanoscience Foundries and Fine Analysis;
STARSED Project (national funding); SiM-SeT Project (MSCA)

Founded by the European Union and the Generalitat de Catalunya under the Beatriu de Pinós program (COFUND 801370 for Marie-Skłodowska-Curie)

CONCLUSIONS AND FUTURE WORK

- Electrically conductive SiNW p-doped devices have been succesfully fabricated.
- Next steps are oriented to study the boron dopping and diffusion after the fabrication process.
- It remains to integrate the gate electrodes to enhance the gateability of the device.
- Finally, low temperature (below 10K) electrical caracteristics will be conducted to study the behaviour of the devices as single electron/hole transistors.

REFERENCES

[1] Llobet J., Sansa M., Gerbolés M., Mestres N., Arbiol J., Borrisé X. & Pérez-Murano F. (2014). Enabling electromechanical transduction in silicon nanowire mechanical resonators fabricated by focused ion beam implantation. Nanotechnology, 25(13), 135302.
[2] Llobet J., Krali E., Wang C., Arbiol J., Jones M.E., Pérez-Murano F. & Durrani Z.A.K (2015). Resonant tunnelling features in a suspended silicon nanowire single-hole transistor. Applied Physics Letters, 107(22), 223501.

Copper oxide nanocubes wrapping metals
by microwave synthesis

Miquel Torras and Anna Roig
Institut de Ciència de Materials de Barcelona, CSIC, Bellaterra, Spain

Abstract

- **The fabrication of noble metal NPs [Au, Ag, Pd, Pt] and Cu_2O heterostructures (HS) by a microwave (MW)-assisted synthesis is presented.**
- MW selectivity with a fast two-step protocol enabled us to easily prepare these multicomponent nanoparticles in a short time (~ 40 min).
- First, metal NPs (Au, Ag, or Pd) are synthesized through a MW-assisted polyol approach and those NPs serve as nucleation seeds for a cubic Cu_2O wrapping.
- Other types of HS were found when using smaller Pt NPs.
- For Au NPs as the core, we analyzed the effect of gold to copper molar ratio on the shape-yield of the nanocubes, reported their optic and plasmonic properties and demonstrated the reproducibility and scalability of the synthetic routes.

Au-Cu_2O HS

Gold to copper molar ratio

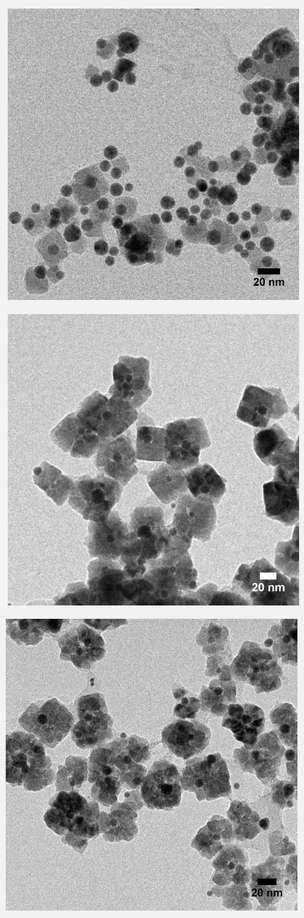

(Increasing gold seeds)

Isolated Au NPs
incomplete shape-oriented formation

Irregular, flower-like structures

HR-TEM

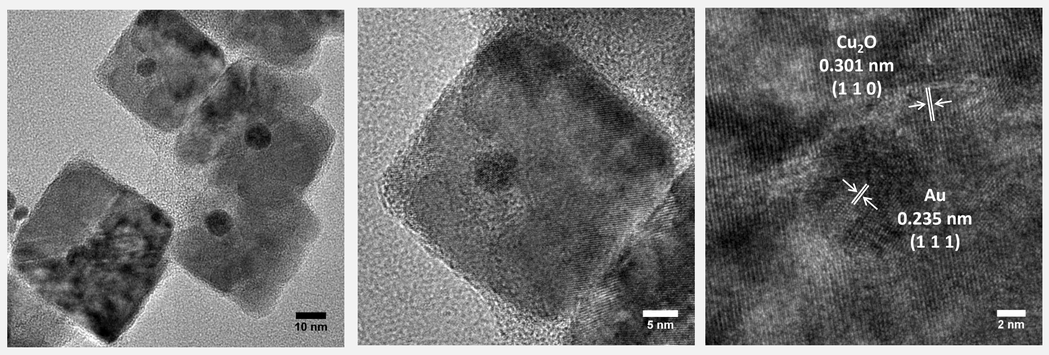

- Cu_2O nanocubes of 30-50 nm edge length wrapping the smaller Au NPs (9 ± 1 nm).
- Homogeneous covering and contact, growth mechanism based on a single cube growth with {1 0 0} facets. No epitaxy relation.

HAADF STEM

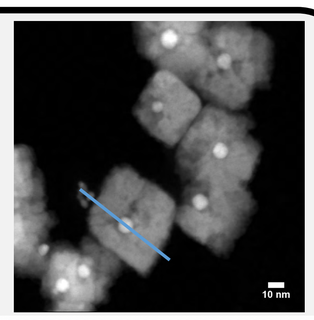

Element profile

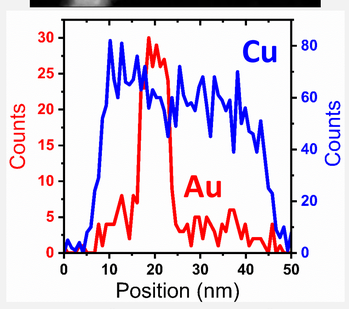

Summary

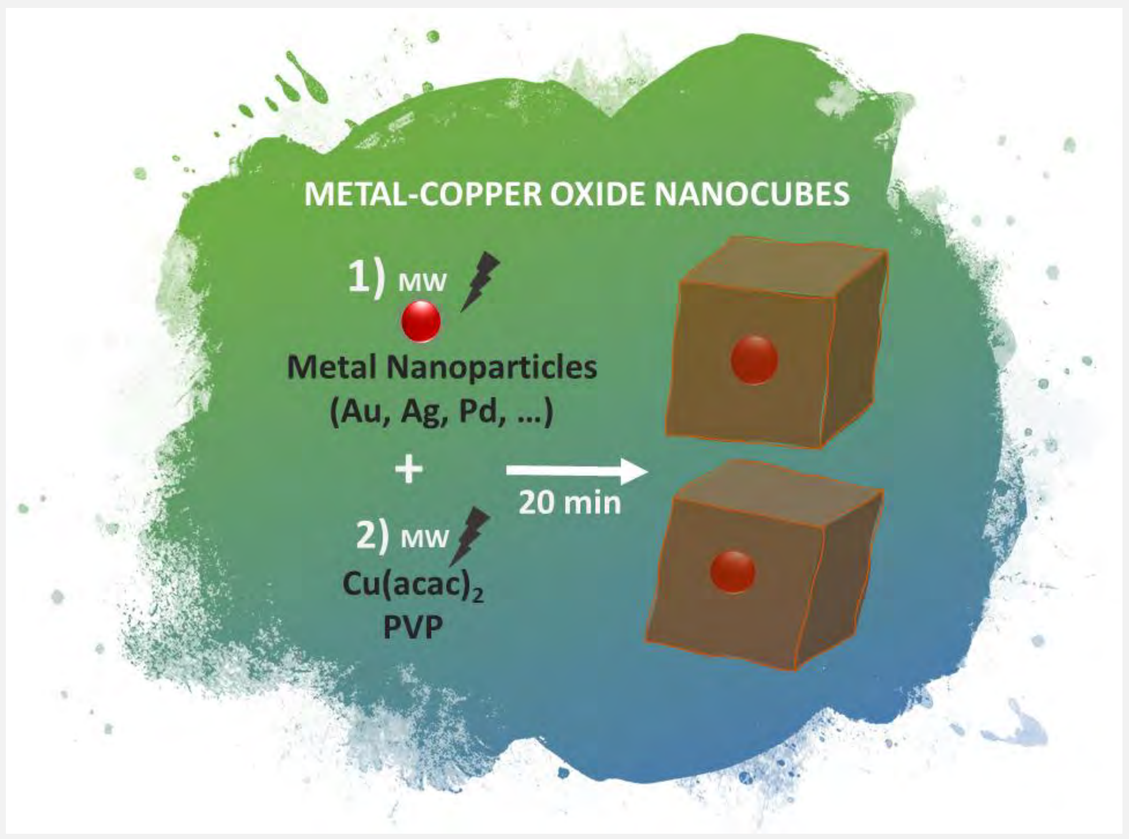

Optic and plasmonic properties

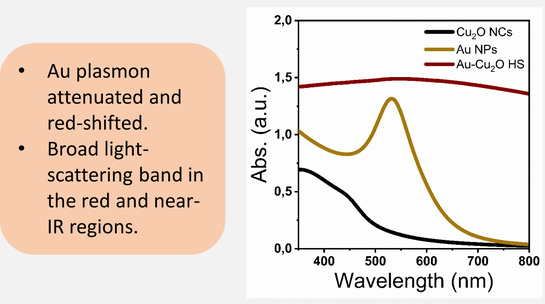

- Au plasmon attenuated and red-shifted.
- Broad light-scattering band in the red and near-IR regions.

Pt-Cu_2O HS

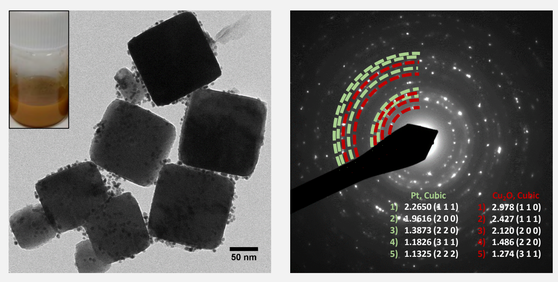

- Cu_2O nanocubes of 100-120 nm edge length with Pt NPs (5 ± 1 nm) attached to the side-facets.

Optic and plasmonic properties

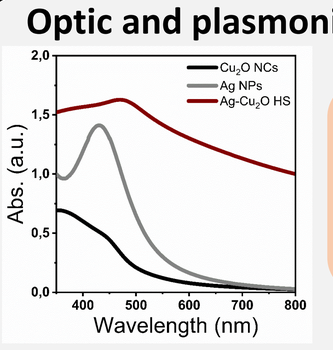

- Ag plasmon attenuated and red-shifted.
- Broad light-scattering band in the red and near-IR regions.

HAADF STEM

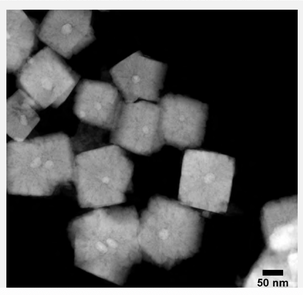

Element profile

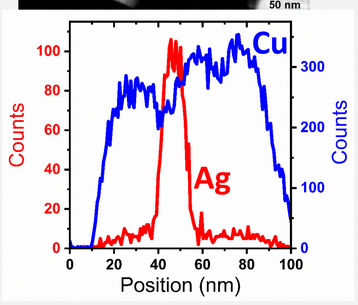

HR-TEM

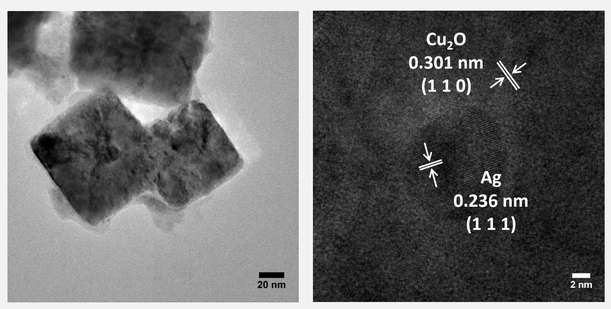

- Cu_2O nanocubes of Cu_2O 60-80 nm edge length wrapping Ag NPs of 13 ± 4 nm.

Ag-Cu_2O HS

TEM

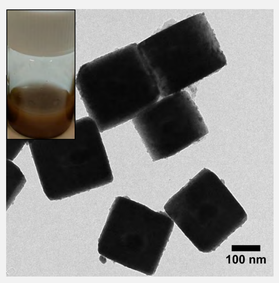

SAED

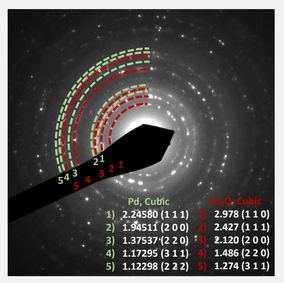

SEM

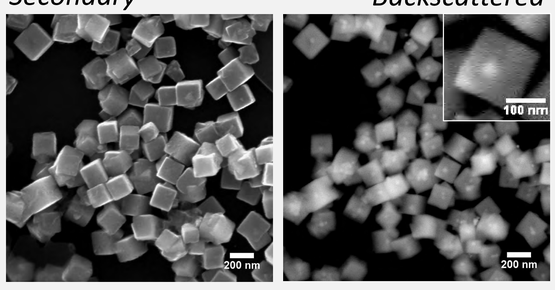

- Cu_2O nanocubes of 150-180 nm edge length wrapping Pd NPs of 50 ± 9 nm.

Pd-Cu_2O HS

M-Cu_2O HS comparison

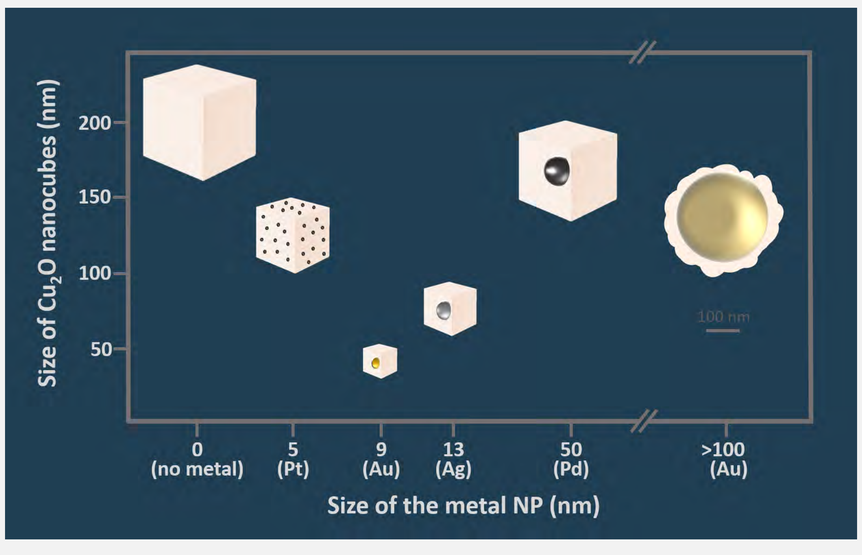

Conclusions

- Noble metal-Cu_2O HS consisting of Cu_2O cubes wrapping a metal core (Au, Ag and Pd) by a universal MW-assisted synthesis have been presented thanks to the MW selectivity and controlling the synthetic parameters such as the molar ratio of metal NPs to $Cu(acac)_2$.
- The overall synthesis time was less than 40 min, no shaping-template agents were used, and the metal-Cu_2O HS were readily dispersible in water.
- With Au NPs used, the HS consisted of Cu_2O cubes ca. 30-50 nm wrapping smaller crystalline Au NPs of ca. 9 nm. HRTEM highlighted a homogeneous covering and contact, indicating a growth mechanism based on a single cube growth with {1 0 0} facets but with no epitaxy relation.
- Regarding optical and plasmonic properties, the spectrum mostly reflected the absorption characteristics of Cu_2O crystals and a broad light-scattering band in the red and near-IR regions, while the characteristic plasmon peak of the Au NPs was attenuated and red-shifted.
- The presented route could be generalized to other metals (Ag and Pd).

https://doi.org/10.1021/acs.cgd.1c00462

Acknowledgements: Ministerio de Educación, Cultura y Deporte (MECD, Spanish Government), FPU grant FPU16/05452 (MT)